

Coincident Learning for Unsupervised Anomaly Detection

Ryan Humble^{1*} Zhe Zhang² Finn O’Shea² Eric Darve¹ Daniel Ratner^{2*}

Abstract

Anomaly detection is an important task for complex systems (e.g., industrial facilities, manufacturing systems, large-scale science experiments), where failures in a sub-system can lead to low yield, faulty products, or even damage to components. While complex systems often have a wealth of data, labeled anomalies are typically rare (or even nonexistent) and expensive to acquire. In this paper, we introduce a new method, called CoAD, for training anomaly detection models on *unlabeled data*, based on the expectation that anomalous behavior in one sub-system will produce coincident anomalies in downstream sub-systems and products. Given data split into two streams s and q (i.e., subsystem diagnostics and final product quality), we define an *unsupervised* metric, \hat{F}_β , out of analogy to the supervised classification F_β statistic, which quantifies the performance of the independent anomaly detection algorithms on s and q based on their coincidence rate. We demonstrate our method in four cases: a synthetic time-series data set, a synthetic imaging data set generated from MNIST, a metal milling data set, and a data set taken from a particle accelerator.

1. Introduction

The problem of anomaly detection, the task of finding abnormal events or data, is an important task for complex systems, such as industrial facilities, manufacturing, and large-scale science experiments (Sun et al., 2016; Zhao et al., 2019; Lutz et al., 2020; Edelen & Cook, 2021; Lindemann et al., 2021; Radaideh et al., 2022). Failures in these systems can lead to low yield, faulty products, or even damage to components, making identifying these failures a high-priority task for system operators. However, the complexity of these systems typically ensures that labeled data is rare

*Equal contribution ¹Institute for Computational and Mathematical Engineering, Stanford University, Stanford, California ²SLAC National Laboratory, Menlo Park, California. Correspondence to: Ryan Humble <ryhumble@stanford.edu>.

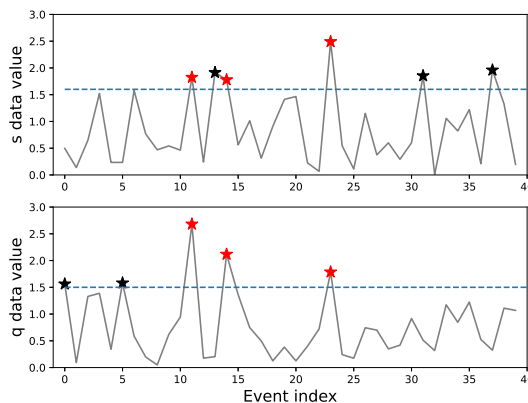


Figure 1. We consider tasks with two data streams, s and q , which should be independent except for anomalous events which exist across both data streams. An anomaly detection algorithm identifies points independently in each stream (stars) using example thresholds (dashed blue line). Events found in only one stream (black stars) are ignored, and only joint events found in both data streams are identified as anomalous (red stars).

or nonexistent and expensive to acquire. This makes traditional supervised classification methods poorly suited to the task of identifying these failures. Even a number of “unsupervised” approaches rely on a completely normal training set (Schlegl et al., 2017; Ruff et al., 2018), which is similarly unavailable for many complex systems. We, therefore, require an *unsupervised* method for detecting anomalies in these complex systems, where the data is inherently polluted by anomalies.

Complex systems are typically broken down into multiple subsystems, all of which impact the overall system performance. We consider the anomaly detection task of identifying an anomalous subsystem (s) in a larger system of connected elements that impact overall system quality (q). The subsystem state is considered anomalous if and only if it impacts the larger system’s overall performance; equivalently, a system issue has only occurred if both the subsystem and larger system experience *coincident* anomalies. Our goal is to leverage the expectation of coincident anomalies between the two data streams, s and q , to classify normal and anomalous examples.

Our motivating example comes from a particle accelerator, for which we have two data streams, one containing data from a radio frequency (RF) station subsystem (s) and one containing electron energy data beam-position monitors (BPMs) that monitor beam quality (q). During normal operation, the variability in the signals is independent (i.e., random fluctuations in s and q are uncorrelated). However, the anomalous behavior of an RF station will have an impact, albeit *unknown*, on the BPM quality data. Even with no ground truth labels for training, we will show that we can exploit the coincidence of abnormalities to determine whether abnormal RF station subsystem behavior has caused beam performance degradation.

1.1. Contributions

In this paper, we consider a subset of anomaly detection tasks in which the input features can be separated into two groups (s and q), for example, drawn from different sources or by partitioning a single source in time or space. Figure 1 demonstrates our problem setting. We assume that the impact of an anomaly is apparent in both sets of features. As a consequence, we expect that there exists an algorithm capable of dividing each data stream into normal and anomalous sets, and crucially the sets should match. Additionally, we assume that s and q data are independent within either the normal or anomalous clusters.

Our main contributions are:

1. We introduce coincident learning for anomaly detection (CoAD) and an unsupervised metric \hat{F}_β , in analogy to the supervised classification metric F_β , that exploits the coincidence between s and q to classify normal and anomalous examples. Specifically, we use two models—taking different data streams as inputs—to classify examples as either normal or anomalous.
2. We also present theoretical results, including showing that our estimate \hat{F}_β is a lower bound of the true F_β under our assumptions and deriving the form of the optimal models under mild conditions. We also interpret our method as an unsupervised representation learner.
3. We show that our metric \hat{F}_β can be used in both a categorical and continuous sense. If the two anomaly detection sub-methods are predefined, \hat{F}_β gives a principled way of selecting the two thresholds (demonstrated in Section 4.1). We can also use \hat{F}_β to train the anomaly detectors end-to-end, with the models parameterized as deep neural networks (DNNs) (demonstrated in Sections 4.2 to 4.4).
4. We demonstrate these contributions on four data sets: a synthetic time-series data set, a synthetic imaging data set generated from MNIST, a publicly available metal

millling data set, and an experimental data set taken from a particle accelerator. For the synthetic cases, we show our unsupervised method performs nearly as well as a supervised counterpart. For the real data sets, we train DNNs end-to-end to achieve data-driven, unlabeled anomaly detection.

2. Coincident Learning

Given a dataset $\mathcal{D} = \{(s, q)\}$ drawn from the respective data streams, we consider a pair of algorithms, $A_{\theta_s}(s)$ and $A_{\theta_q}(q)$, parameterized by θ_s and θ_q . The algorithms will each have a scalar output, $p_s, p_q \in [0, 1]$, which we will interpret as the confidence that the example belongs to the anomalous class. Let $\mathcal{D}_s = \{s\}$ and $\mathcal{D}_q = \{q\}$ be the marginal datasets for s and q respectively. Also, we assume that the data is generated from an unseen state variable x (i.e., both are functions of x : $s(x)$ and $q(x)$). We present a schematic of our method in Figure 2.

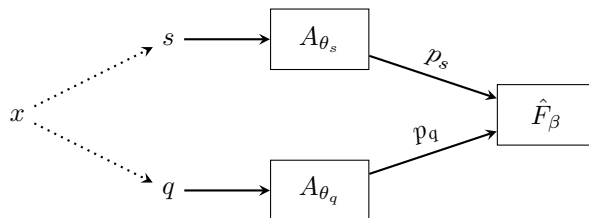


Figure 2. A schematic of CoAD showing the two data streams s and q (generated from a hidden state x) and their respective algorithms A_{θ_s} and A_{θ_q} , which are trained to maximize our unsupervised metric \hat{F}_β .

2.1. CoAD Objective

To begin, we restrict ourselves to the case where p_s and p_q are categorical labels in $\{0, 1\}$. We define a *joint event* as one where both algorithms classify the respective data as anomalous, i.e., $p_{s,i} = p_{q,i} = 1$. Since we lack true labels, we cannot determine which joint events are true positives (true anomalous events) or are false positives (normal events flagged as anomalies). However, we show below that we can estimate the number of false positives from the disagreement between the two algorithms. We can then compare the actual number of observed joint events with the estimated number of false positive events to measure the efficacy of the algorithms. The more joint events we observe, the more sensitive our algorithm. The fewer points with conflicting predictions (and thus fewer estimated false positives), the more precise our algorithm.

Let $J(\theta_s, \theta_q)$ denote the fraction of joint events found in our data (i.e., predicted positives). Suppose α is the anomaly fraction in our data (i.e., actual positives). If we had labels for each of the n examples in our dataset, we would evaluate

our algorithm with the supervised metric F_β , which can be written as

$$F_\beta = \frac{(1 + \beta^2)(J - \text{FP}/n)}{J + \alpha\beta^2},$$

where higher values are better, FP is the number of false positives, and β balances the weighting of precision and recall. However, since we lack labels, we will rely on an estimate $D(\theta_s, \theta_q)$ of the fraction of false positives. (We also show later an estimate of α suffices.) We therefore recover an unsupervised version \hat{F}_β :

$$\hat{F}_\beta = \frac{(1 + \beta^2)(J - D)}{J + \alpha\beta^2}.$$

The quantity \hat{F}_β can now be used to compare algorithms or select model hyperparameters in the same manner as its supervised counterpart. As in the supervised case, the extremes are $\hat{P} = \hat{F}_0$ and $\hat{R} = \hat{F}_\infty$, which correspond to precision P and recall R . We can use \hat{F}_β to pick a model that strikes a balance between the number of anomalous events found (maximizing the recall) and the confidence in the prediction (maximizing precision).

The \hat{F}_β definition requires an estimate of the fraction of false positives $D(\theta_s, \theta_q)$. Our strategy is based on an observation that *disagreements* between A_{θ_s} and A_{θ_q} reveal the false positive rate of the individual algorithms. Under the assumption that s and q are independent conditioned on knowing the true label, Theorem 2.1 shows that the disagreement rates provide an upper bound on the true fraction of false positives. (All proofs are deferred to the Appendix.)

Theorem 2.1. *Assume that s and q are independent conditioned on knowing the true label, and assume that the algorithms $A_{\theta_s}, A_{\theta_q}$ are no worse than random guessers. Define $D(\theta_s, \theta_q) = \mathbb{E}_{(s,q) \in \mathcal{D}}[p_s | \neg p_q] \mathbb{E}_{(s,q) \in \mathcal{D}}[p_q | \neg p_s]$ to be our estimated fraction of false positives. Then, in the categorical case, the fraction of false positives is no more than D and the fraction of true positives is at least $J - D$, implying that \hat{R}, \hat{P} , and \hat{F}_β are lower bounds of their supervised counterparts R, P , and F_β .*

Corollary 2.2. *Additionally define $D_{\text{naive}}(\theta_s, \theta_q) = \mathbb{E}_{s \in \mathcal{D}_s}[p_s] \mathbb{E}_{q \in \mathcal{D}_q}[p_q]$, which is equivalent to an assumption that s and q are completely independent. Then, $D(\theta_s, \theta_q) \leq D_{\text{naive}}$.*

Therefore, by definition of a joint event and the conditional expectation, the fraction of joint events in the data and the estimated fraction of false positives are

$$J(\theta_s, \theta_q) = \mu_{sq} \quad (1)$$

$$D(\theta_s, \theta_q) = \frac{\mu_s - \mu_{sq}}{1 - \mu_q} \frac{\mu_q - \mu_{sq}}{1 - \mu_s}, \quad (2)$$

where $\mu_s = \mathbb{E}_{s \in \mathcal{D}_s}[p_s]$, μ_q similarly, and $\mu_{sq} = \mathbb{E}_{(s,q) \in \mathcal{D}}[p_s p_q]$. This allows us to concretely write our unsupervised metric as

$$\hat{F}_\beta = (1 + \beta^2) \frac{\mu_{sq} - \mu_s \mu_q}{\mu_{sq} + \alpha\beta^2} \frac{1 - \mu_{sq}}{(1 - \mu_s)(1 - \mu_q)}. \quad (3)$$

It is crucial to note that we implicitly require a majority of the events to be labeled as 0, or equivalently require the anomalous class to be the minority class; this is a necessary condition since precision and recall (and our unsupervised analogues) are not invariant under a labeling flip. Thus, we additionally impose the constraint that anomalies exist and are rare ($0 < \mu_{sq} \leq \mu_s, \mu_q \leq 0.5$). Also, as a point of optimization, it might appear that maximizing \hat{F}_β requires that both α and β be defined. However, as $1 + \beta^2$ is just a constant scalar, we need only specify the quantity $\alpha\beta^2$. If we used an incorrect estimate of α (since the true α is unknown), we have merely maximized our metric for a different value of β . Moreover, the maximizers of \hat{P} and \hat{R} do not depend on α at all.

Lastly, when developing our metric, we assumed the categorical case ($p_s, p_q \in \{0, 1\}$). This case might naturally arise when the two algorithms $A_{\theta_s}, A_{\theta_q}$ already exists and are parameterized by two thresholds. The metric then allows a principled way of setting these thresholds, as we demonstrate in Section 4.1. But notably, our metric naturally extends to the case of continuous $p_s, p_q \in [0, 1]$. This allows us to train more complex algorithms $A_{\theta_s}, A_{\theta_q}$, such as ones parameterized as DNNs and trained with gradient-based optimizers, thereby allowing us to cluster normal and anomalous data without having to first build the individual anomaly detection algorithms. We present a theoretical justification for the continuous extension in the following section.

2.2. Properties of CoAD

Under certain simplifying assumptions, we can derive results regarding the solution to the optimization problem. Throughout we assume that $p_s(s) = A_{\theta_s}(s)$, for some choice of parameters θ_s , can map D_s to any element of $[0, 1]^n$ where n is the number of samples in the training set (and similarly for $p_q(q) = A_{\theta_q}(q)$).

We first consider the possible forms of the maximizers p_s^*, p_q^* of \hat{F}_β . Holding p_s fixed, Theorem 2.3 shows that the optimal p_q^* is (nearly) categorical: $p_q^*(q) \in \{0, \rho, 1\}$ for some $\rho \in [0, 1]$ and all q . Moreover, Theorem 2.4 shows $\rho \notin \{0, 1\}$ only occurs if the constraint $\mu_q \leq 0.5$ is tight. By applying this twice (first for fixed p_s and then again with the new p_q fixed), we need only consider (nearly) categorical solutions for p_s, p_q . Thus, the continuous extension (to $p_s, p_q \in [0, 1]$) is almost equivalent to the original categorical case, and our method behaves as a (nearly) hard clustering algorithm.

Theorem 2.3. Assume θ_s is fixed (with $\mu_s \in (0, 0.5]$). Let $w(q) = \mathbb{E}_{s|q \in \mathcal{D}_{s|q}}[p_s(s)]$. Then, the maximum of \hat{F}_β can be achieved by a (nearly) categorical solution: $p_q^*(q) = \mathbf{1}\{w(q) > \tau\} + \rho \mathbf{1}\{w(q) = \tau\}$ for some $\rho, \tau \in [0, 1]$.

Theorem 2.4. Additionally, a non-categorical solution (i.e., with $\rho \notin \{0, 1\}$) can only be uniquely optimal if the constraint $\mu_q \leq 0.5$ is tight.

Armed with the optimal form of p_s, p_q , we now derive the solution for the illustrative scenario shown in Figure 3. We specifically consider when the anomalous and normal sets, respectively A and A^c , might overlap in the data streams s and q (i.e., the data streams s and q can be noisy). Theorem 2.5 shows that, under some mild conditions, the optimal solution always labels the noiseless parts of s and q according to their true cluster labels: $p_s(s(A \setminus B)) = p_q(q(A \setminus C)) = 1$ and $p_s(s(A^c \setminus B)) = p_q(q(A^c \setminus C)) = 0$. The noisy part of q (i.e., the set C) is always labeled as anomalous, but the label for the noisy part of s (i.e., the set B) depends on the setting of β . Choosing $\beta = 0$ (i.e., $\hat{F}_0 = \hat{P}$) prioritizes precision, so the optimal solution does not assign the noisy examples in B to the anomalous class; choosing $\beta = \infty$ (i.e., $\hat{F}_\infty = \hat{R}$) prioritizes recall, so the optimal solution labels B as anomalous. This tradeoff occurs abruptly at a critical β_{crit} that depends on the noise level in both s and q .

Theorem 2.5. Suppose the variable x exists in some probability space $(\Omega, \mathcal{F}, \mathbb{P})$. As depicted in Figure 3, denote $A \in \mathcal{F}$ and A^c its complement, where $\alpha = \mathbb{P}(A) \leq 0.5$. Assume (i) $s(A) \cap s(A^c) = s(B)$ and $q(A) \cap q(A^c) = q(C)$; (ii) s and q are independent when $x \in A$ (and similarly when $x \in A^c$); (iii) $\mathbb{P}(A \cup B), \mathbb{P}(A \cup C) \leq 0.5$; (iv) $\mathbb{P}(A \setminus B \setminus C) > 0$; (v) $\mathbb{P}(A^c \setminus B \setminus C) \geq \mathbb{P}(A^c \setminus B)\mathbb{P}(A^c \setminus C)$; and (vi) $\mathbb{P}(A^c \setminus B \setminus C)\mathbb{P}(A \setminus C) \geq \mathbb{P}(A \setminus B \setminus C)\mathbb{P}(A^c \setminus C)$. Wlog let $\mathbb{P}(A \setminus B) \geq \mathbb{P}(A \setminus C)$. Then the maximum of \hat{F}_β is achieved when

$$\begin{aligned} p_s(s(A \setminus B)) &\equiv 1, & p_q(q(A \setminus C)) &\equiv 1, \\ p_s(s(A^c \setminus B)) &\equiv 0, & p_q(q(A^c \setminus C)) &\equiv 0, \\ p_s(s(B)) &\equiv \mathbf{1}\{\beta^2 \geq \beta_{\text{crit}}^2\}, & p_q(q(C)) &\equiv 1. \end{aligned}$$

where β_{crit} depends on the sets A, A^c, B , and C .

Lastly, in the case where both algorithms $A_{\theta_s}, A_{\theta_q}$ are parameterized as DNNs, we note that our method performs both feature representation and classification, simultaneously and in an unsupervised manner. Suppose the final components of each DNN are a fully-connected (FC) layer and a sigmoid activation. The final layer and sigmoid then amount to a logistic classifier on the latent representations (i.e., representation fed to the final FC layer). The backbones of the networks are then tasked with learning how to generate linearly-separable representations of the input data. Theorem 2.6 shows the gradients with respect to the

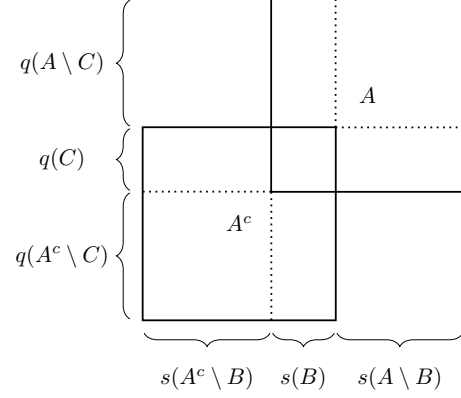


Figure 3. An illustrative, noisy anomaly scenario. Setting of Theorem 2.5.

logistic classifier parameters w_s, b_s and the latent representations $z_s(s)$, and illustrates several important qualitative behaviors. First, the gradients depend *most* on the uncertain examples $p_s(s)$ and ignore examples with high confidence, as $\gamma_s(s) = 0$ for $p_s(s) \in \{0, 1\}$, meaning the examples on the “margin” are most important. Second, the gradients also depend on the pseudo-target $\hat{y}_q(q)$, which has largest magnitude for the most certain examples $p_q(q)$. Taken together, the \hat{F}_β metric encourages each individual algorithm to adopt the other’s prediction when it is uncertain but the other algorithm is confident.

Theorem 2.6. Suppose p_s, p_q are parameterized as DNNs, whose final components of each DNN are a fully-connected layer and a sigmoid activation. Let the latent representation fed into the final layer be $z_s(s), z_q(q) \in \mathbb{R}^p$ for the two networks respectively. Define $p_s(s) = \sigma(w_s^T z_s(s) + b_s)$ and $p_q(q) = \sigma(w_q^T z_q(q) + b_q)$. Then,

$$\begin{aligned} \nabla_{w_s} \hat{F}_\beta &\equiv \mathbb{E}_{\mathcal{D}}[\hat{y}_q(q) \gamma_s(s) z_s(s)] \\ \nabla_{b_s} \hat{F}_\beta &\equiv \mathbb{E}_{\mathcal{D}}[\hat{y}_q(q) \gamma_s(s)] \\ \nabla_{z_s(s)} \hat{F}_\beta &\equiv \mathbb{E}_{\mathcal{D}_{q|s}}[\hat{y}_q(q) \gamma_s(s) z_s(s)] \end{aligned}$$

where $\hat{y}_p(p) = c_1 p_q(q) - c_2$ and $\gamma_s(s) = p_s(s)(1 - p_s(s))$. The gradients w.r.t. the q network are analogous. The constants c_1, c_2 depend on the current parameters θ_s, θ_q but not individual instances $(s, q) \in \mathcal{D}$. If the networks are better than random guessers, then $c_1, c_2 \geq 0$.

3. Related Work

3.1. Unsupervised anomaly detection

Our method falls into an extremely large body of work identifying anomalies in unsupervised (or semi-supervised “normal-only”) data. The most popular classical methods, such as One-Class SVM (OCSVM) (Schölkopf et al., 2001), Isolation Forest (Liu et al., 2008), Local Outlier Factor (Bre-

unig et al., 2000), and Kernel Density Estimation (Parzen, 1962), typically suffer from the curse of dimensionality. These methods struggle with high dimensional inputs primarily for two reasons: (i) they rely on distances in high-dimension; and (ii) they require feature engineering because their possible decision boundaries are limited. Since we can leverage DNNs, our approach suffers from neither and can represent the normal and anomalous sets using complex decision boundaries. Many recent works, such as DSVDD (Ruff et al., 2018), RandNet (Chen et al., 2017), and AnoGAN (Schlegl et al., 2017), also leverage DNNs for these reasons. However, these approaches assume either (i) the training data is completely “normal” or (ii) the anomalies exist in low-density regions. Our method does not make these assumptions; in fact, we explicitly assume our data is polluted by anomalies, which are quite possibly densely clustered (for example, repeated failures might have extremely similar signatures).

3.2. Common representation learning

In the absence of labels for classification, many prior works have proposed unsupervised methods for learning feature representations of different views (or modalities) of the data. A key concept behind these approaches is to maximize the alignment between the feature representations.

Perhaps the best known approach uses Canonical Correlation Analysis (CCA) (Hotelling, 1936) (or a kernel generalization (Akaho, 2006)) to create similar feature representations for multiple views (Hardoon et al., 2004). There are a large number of variants and applications, most notably a deep neural network adaptation called Deep Canonical Correlation Analysis (DCCA) (Andrew et al., 2013). In the notation of our paper, DCCA proposes an objective $\max_{\theta_s, \theta_q} \text{Corr}(A_{\theta_s}, A_{\theta_q})$ where the algorithms are parameterized as DNNs and the outputs are not necessarily in $[0, 1]$. Both DCCAE (Wang et al., 2015) and CorrNet (Chandar et al., 2016) build upon this idea and add autoencoders to the formulation.

Our method differs in several respects. First, we apply our \hat{F}_β objective to a single dimensional output p_s, p_q from each algorithm; this is required since we are interpreting the final output as an anomaly probability. DCCA, DCCAE, and CorrNet predict into a multi-dimensional latent space to achieve higher correlation. Second, the correlation objective is scale invariant. Suppose that p_s^*, p_q^* are the maximizers of the correlation objective; then any ap_s^*, bp_q^* for $ab > 0$ is also a maximizer. This is problematic for interpreting the output as an anomaly label, as the scale of the p_s, p_q is free and can be arbitrarily small. Lastly, the correlation objective is qualitatively similar to the special case $\hat{F}_0 = \hat{P}$ of our method, in that they both promote maximum precision and are agnostic to the number of anomalies found. This

behavior of \hat{P} (and correlation) is why the control over β (i.e., between \hat{P} and \hat{R}) is desirable.

The other common representation learning approach uses a covariance-based objective for learning common feature representations. If the two views of the data are the same, this is in fact what principal component analysis (PCA) optimizes for. For different views, maximum covariance analysis (MCA) (Storch & Zwiers, 1999) (also known as SVD analysis (Bretherton et al., 1992; Wallace et al., 1992)) maximizes the covariance between linear projections of the two views. Deep Maximum Covariance Analysis (DMCA) (Luo et al., 2018) allows for deeper, nonlinear projections (parameterized by neural networks) within the same covariance framework. In the notation of our paper, DMCA proposes an objective $\max_{\theta_s, \theta_q} \text{Cov}(A_{\theta_s}, A_{\theta_q})$ and is otherwise identical to DCCA. This covariance objective is qualitatively similar to the special case $\hat{F}_\infty = \hat{R}$, in that they both promote maximum recall. Specifically, we have

$$\hat{R} = \frac{1}{\alpha} \text{Cov}(p_s, p_q) \frac{1 - \mu_{sq}}{(1 - \mu_s)(1 - \mu_q)}$$

The last term is always at least 1 (since $0 < \mu_{sq} \leq \mu_s, \mu_q$). Thus, under the assumption that s and q are independent given the true label (see Theorem 2.1), we have $\frac{1}{\alpha} \text{Cov}(p_s, p_q) \leq \hat{R} \leq R$ where R is the true recall. This is also a natural conclusion of Corollary 2.2, which shows that we would have recovered covariance if we had instead made the assumption that s and q are completely independent. Equivalently, covariance measures the number of joint events in excess of those that would have occurred simply by chance, which has a connection to Cohen’s kappa (Cohen, 1960). Therefore, in our setting, covariance can only be a worse underestimate of the recall (i.e., number of anomalies) than our metric \hat{R} . We show this for a synthetic example in Section 4.1.

3.3. Self-supervision

It may also be useful to view our method through the concepts of self-supervision. In contrastive self-supervision, an algorithm (for example by augmentation) labels examples as either similar (“positive”) or dissimilar (“negative”). The contrastive loss function then encourages the network to map positive examples close to each other and negative examples far apart. Our approach is most similar to that of SimCLR (Chen et al., 2020), which applies a contrastive-type loss to learn representations of images; it uses different transformations of the same image as “positive” examples and the other examples in the training batch as “negative” examples. We assume our data is already paired into (s, q) “positive” pairs and similarly use the training batch as the “negative” examples through the penalty on the estimated number of false positives D . Our metric can therefore be interpreting as encouraging similar labeling (through μ_{sq})

while preventing mode collapse (through D , which sends \hat{F}_β to zero if all labels are identical). Unlike SimCLR, our approach does not require the transformations to be specified and is applicable to multi-modal data or non-Siamese networks.

4. Experiments

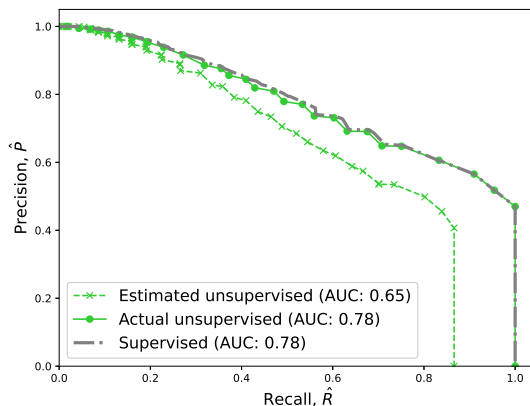
We assess our method on several test cases, in both the categorical and continuous settings. In the continuous setting, we train our DNNs using the PyTorch framework (Paszke et al., 2019), Adam optimizer (Kingma & Ba, 2015), mini-batches, and a sigmoid-based regularizer to enforce the constraint $\mu_s, \mu_q \leq 0.5$. Full details on the training settings and architectures can be found in the Appendix.

4.1. Synthetic time-series outliers

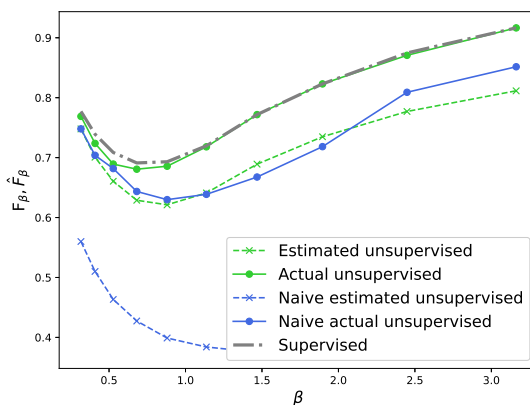
We start by illustrating the categorical case. We create a synthetic dataset of 20k normal points sampled from $|\mathcal{N}(0, 1)|$ for both s and q . We then introduce anomalies by sampling from $1 + |\mathcal{N}(0, 1.5)|$ for 5% of the data points. Anomalies always occur simultaneously in both data streams. We then use a simple threshold as the anomaly detection algorithm, applied independently to each data stream, and identify as anomalous any point that exceeds the threshold simultaneously in both s and q . This setup corresponds to pre-specified algorithms $A_{\theta_s}, A_{\theta_q}$ where the parameters are just single thresholds on the algorithm outputs. Figure 1 illustrates a small example.

To evaluate our approach, we first determine the estimated \hat{P} - \hat{R} curve and the s and q thresholds that define it. Since the assumptions of Theorem 2.1 are met for this synthetic case, \hat{R}, \hat{P} are underestimates of recall R and precision P , respectively, for any choice of thresholds. As we have ground truth labels, we can calculate the actual precision and recall values defined by the same unsupervised s and q thresholds; we denote this curve the ‘‘actual unsupervised’’ curve. As a reference, we also find the supervised P - R curve using the labels (i.e., find the optimal s and q thresholds directly using the labels). Figure 4(a) shows these three precision-recall curves - estimated, actual, and supervised - where we plot \hat{R}, \hat{P} for the estimated case. Although our method is unsupervised, the actual precision-recall curve almost exactly matches the supervised precision-recall curve.

We can also analyze \hat{F}_β and the thresholds that maximize it, for a range of β . As above, we have the estimated \hat{F}_β curve and the actual F_β curve using the same unsupervised thresholds. To illustrate our method for estimating the fraction of false positives, we compare the definitions given in Theorem 2.1 and Corollary 2.2. We denote the latter definition, D_{naive} , as the ‘‘naive’’ rate. Using the ground truth, we also calculate the supervised F_β curve. Figure 4(b)



(a) Comparison of the supervised precision-recall curve to the estimated \hat{P} - \hat{R} curve.



(b) Comparison of supervised F_β to estimated \hat{F}_β , found using two different estimates for the fraction of false positives.

Figure 4. Analysis of our unsupervised method on a synthetic dataset. The ‘‘actual’’ curves use the optimal thresholds from the estimated curves but evaluate using the ground truth labels.

shows the five curves—‘‘estimated unsupervised’’, ‘‘actual unsupervised’’, ‘‘naive estimated unsupervised’’, ‘‘naive actual unsupervised’’, and ‘‘supervised’’—where we plot \hat{F}_β for the estimated cases. While both estimates of the false positive fraction lead to underestimates of \hat{F}_β , our definition $D(\theta_s, \theta_q)$ gives a significantly better estimate than D_{naive} and the corresponding ‘s’ and ‘q’ thresholds achieve near supervised-level performance when assessed with the ground truth labels.

4.2. MNIST

As a second example, we construct an imaged-based anomaly detection task using MNIST. Each example consists of a pair of images, one given as input to each network.

Normal examples consist of a pair of images of the digit 0. Anomalous examples are pairs of images drawn from the digits 1, 2, or 3, with the same digit given to each network (i.e., there are 3 different anomaly types). We then alter the difficulty by imposing a noisy observation model, where with some probability the image fed to each network is replaced by another digit, such that each anomaly class has different amounts of noise (1 having the least noise and 3 having the most noise). The full observation model is detailed in the Appendix.

Table 1. Fraction of MNIST digits labeled as anomalous under a noisy observation model. A digit is labeled anomalous if the product of the two network outputs is greater than 0.5. Results are shown for several different values of β and rounded to the nearest tenth of a percent.

	$\beta = 0.01$	$\beta = 1$	$\beta = \infty$
Digit 0	0%	0.5%	0.5%
Digit 1	86.3%	99.1%	100%
Digit 2	0%	96.9%	99.2%
Digit 3	0.2%	1.2%	99.6%

Table 1 shows the results for different values of β . In particular, we illustrate that different choices of β result in classifying different sets of anomalies: small β only identifies the least noisy anomalies, and large β identifies all 3 anomaly classes. The full violin plots are shown in the Appendix. We can also visualize the latent representations created by the algorithms A_{θ_s} and A_{θ_q} . Despite being trained without labels, our method learned to separate the digits, as shown in Figure 5.

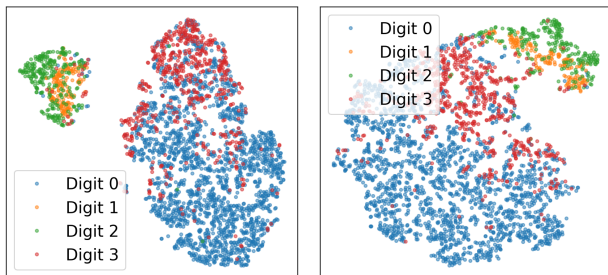


Figure 5. t-SNE (van der Maaten & Hinton, 2008) visualization of the latent representations of the MNIST digits. We show the representations of A_{θ_s} (left) and A_{θ_q} (right) for $\beta = 1$.

4.3. Milling dataset

We now demonstrate our method on a real-world dataset. The University of California, Berkeley Milling dataset (Agogino & Goebel, 2007) is an open dataset of acoustic, vibration, and current measurements from a set

of metal milling cuts. A recent paper (Hahn & Mechefske, 2021) provides a detailed description of the task, analysis code, and results from a variational autoencoder (VAE). The dataset consists of 167 different milling cuts, corresponding to a total of approximately 100 minutes of milling. There are six total diagnostics: acoustics and vibrations from the spindle, acoustics and vibration from the table, and AC and DC current. In addition, the degree of flank wear on the milling tool is measured after a selection of the cuts. We follow the task as described in (Hahn & Mechefske, 2021), breaking the data into 0.25 second chunks, and try to predict whether the milling performance in each chunk is “healthy” or “degraded/failed,” with the label determined by the degree of flank wear.

To apply coincident learning to the milling task, we divide the diagnostics into two sets: acoustics and vibration measurements (four data streams) and AC/DC current measurements (two data streams). (Note that in the milling dataset there is not a default separation into “subsystem” and “quality” measurements.) Also, in part because the “degraded/failed” examples are the majority case, our algorithm learns to identify the most “healthy” examples as a distinct class. Figure 6 shows the predictions from the networks trained under coincident learning (at $\beta = 6$) as compared to the predictions from the VAE of (Hahn & Mechefske, 2021). Our model has perfect predictions on failed examples while identifying more “healthy” and “degraded” examples as anomalous compared to the VAE. We emphasize that in contrast to the VAE, the coincident model does not require training only on “healthy” data.

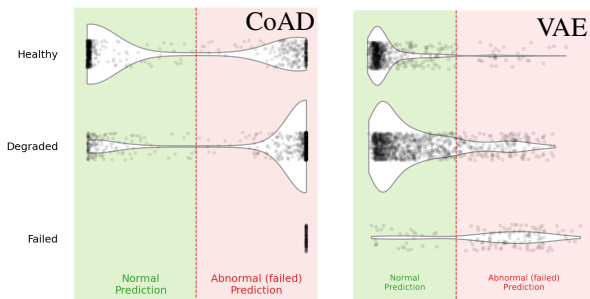


Figure 6. Milling data set results. (Left) Violin plot showing predictions from the \hat{F}_6 model; the prediction values are the products of the two network outputs. (Right) Violin plot showing predictions from the VAE in (Hahn & Mechefske, 2021).

The labels defined in (Hahn & Mechefske, 2021) are quite simplistic, using only the degree of flank wear and ignoring the other milling parameters: metal type, cut speed, and cut depth. While the flank wear is indicative of milling performance, the amount of wear that will lead to anomalous milling may differ across these different milling settings. Figure 7 shows the model’s anomaly confidence versus

the flank wear for two different milling configurations (the other six are shown in the Appendix). There is only a weak correlation between our predictions and flank wear in *aggregate* across all eight milling settings but a very strong correlation for each *individual* configuration. We emphasize that the models never see the flank wear measurements or milling configurations during training, and are trained simultaneously on all milling configurations. We infer that the simplistic labels based on flank wear alone may be incorrect.

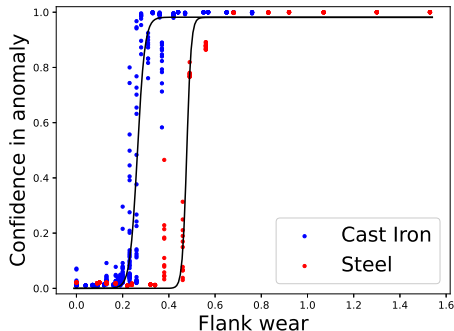


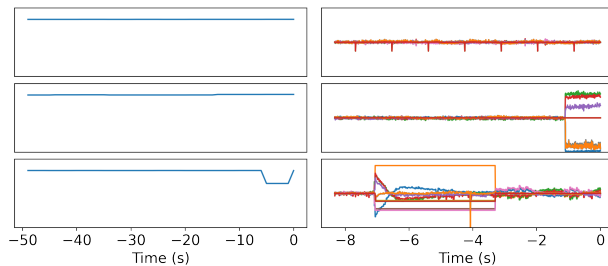
Figure 7. Anomaly probability versus flank wear for two different milling configurations (cast iron (left) and steel (right) at 0.75mm cut depth and 0.25mm/rev cut speed). Black lines are sigmoid fits.

4.4. Particle accelerator RF stations

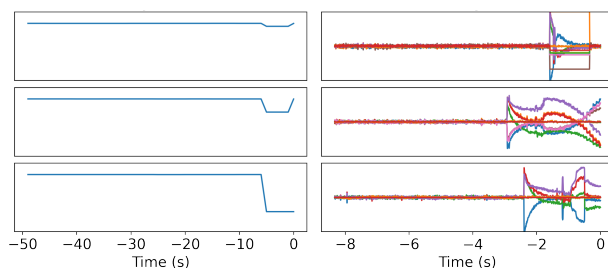
We now return to our original motivating problem of identifying the source of RF station faults. We utilize the dataset assembled and described in (Humble et al., 2022). The subsystem (s) data stream consists of time-series data for a single RF station, with one data point approximately every 5 seconds. We use a sensitive trigger to actively select time windows with the possibility of an event to reduce data requirements; any relative change of 0.5% will trigger a window to be acquired. The quality (q) data stream consists of beam-position monitor (BPM) data from seven different BPM diagnostics in dispersive (i.e., energy-sensitive) regions of the accelerator. Each BPM stream consists of beam positions in the dispersive direction, recorded synchronously at 120 Hz. Time windows are selected to cover the 8 seconds prior to the end of each (asynchronous) RF station event.

Figure 8 shows examples identified as normal and anomalous. Many of the anomalous cases are apparent by eye. For the normal cases, we specifically selected non-trivial examples that a non-expert might identify as abnormal, but which upon close examination does not correspond to an anomaly in the selected RF station data. For example, the final normal case even contains an abnormal energy deviation, but the algorithm correctly determines that the BPM abnormality is too early compared to the RF station anomaly (as described

in (Humble et al., 2022)). We note that with significant effort, it is possible to design hand-tailored anomaly detection algorithms for each data stream, as in (Humble et al., 2022), through manual inspection. However, the NN approach has zero manually set parameters and avoids the need for a hand-designed anomaly detection algorithm. Evaluating using the ground truth labels, our NN achieves a F_1 score of 0.86, compared to 0.9 for the hand-tailored algorithms (within the expected error rate of the hand labels). For accelerators, the NN approach can scale to cover thousands of potential anomaly sources.



(a) Normal examples



(b) Anomalous examples

Figure 8. Experimental RF station data examples. Each example shows both the RF station (left) and electron BPM (right) streams.

5. Conclusion

This work presents a new unsupervised method for detecting coincident anomalies in two data streams. We use the disagreement between two anomaly detection algorithms, one for each set of data, to eliminate the need for labels. We derive several theoretical properties of our metric \hat{F}_β , revealing it as a type of clustering algorithm whose behavior is configurable with β . Moreover, when the algorithms are DNNs, we show that our method simultaneously performs representation learning and clustering. Although we only consider a single value of β when optimizing \hat{F}_β in this work, our approach can be generalized to optimizing an entire frontier of choices simultaneously, allowing for the representation backbone to be reused. Lastly, we demonstrated that our method achieves near supervised-levels of performance on several data sets—synthetic and real, time-series and image-based.

References

- Agogino, A. and Goebel, K. Milling data set. NASA Ames Prognostics Data Repository, NASA Ames Research Center, Moffett Field, CA, 2007.
- Akaho, S. A kernel method for canonical correlation analysis, 2006. URL <https://arxiv.org/abs/cs/0609071>.
- Andrew, G., Arora, R., Bilmes, J., and Livescu, K. Deep canonical correlation analysis. In Dasgupta, S. and McAllester, D. (eds.), *Proceedings of the 30th International Conference on Machine Learning*, number 3 in *Proceedings of Machine Learning Research*, pp. 1247–1255, Atlanta, Georgia, USA, 17–19 Jun 2013. PMLR. URL <https://proceedings.mlr.press/v28/andrew13.html>.
- Bretherton, C. S., Smith, C., and Wallace, J. M. An intercomparison of methods for finding coupled patterns in climate data. *Journal of Climate*, 5(6):541–560, jun 1992. doi: 10.1175/1520-0442(1992)005<0541:aiomff>2.0.co;2. URL <https://doi.org/10.1175%2F1520-0442%281992%29005%3C0541%3Aaiomff%3E2.0.co%3B2>.
- Breunig, M. M., Kriegel, H.-P., Ng, R. T., and Sander, J. LOF. *ACM SIGMOD Record*, 29(2):93–104, may 2000. doi: 10.1145/335191.335388. URL <https://doi.org/10.1145%2F335191.335388>.
- Chandar, S., Khapra, M. M., Larochelle, H., and Ravindran, B. Correlational neural networks. *Neural Computation*, 28(2):257–285, feb 2016. doi: 10.1162/neco.a_00801. URL https://doi.org/10.1162%2Fneco_a_00801.
- Chen, J., Sathe, S., Aggarwal, C., and Turaga, D. Outlier detection with autoencoder ensembles. In *Proceedings of the 2017 SIAM International Conference on Data Mining*, pp. 90–98. Society for Industrial and Applied Mathematics, jun 2017. doi: 10.1137/1.9781611974973.11. URL <https://doi.org/10.1137%2F1.9781611974973.11>.
- Chen, T., Kornblith, S., Norouzi, M., and Hinton, G. A simple framework for contrastive learning of visual representations. In III, H. D. and Singh, A. (eds.), *Proceedings of the 37th International Conference on Machine Learning*, volume 119 of *Proceedings of Machine Learning Research*, pp. 1597–1607. PMLR, 13–18 Jul 2020. URL <https://proceedings.mlr.press/v119/chen20j.html>.
- Cohen, J. A coefficient of agreement for nominal scales. *Educational and Psychological Measurement*, 20(1):37–46, 1960. doi: 10.1177/001316446002000104. URL <https://doi.org/10.1177/001316446002000104>.
- Edelen, J. P. and Cook, N. M. Anomaly detection in particle accelerators using autoencoders. *arXiv preprint arXiv:2112.07793*, 2021.
- Hahn, T. V. and Mechefske, C. K. Self-supervised learning for tool wear monitoring with a disentangled-variational-autoencoder. *International Journal of Hydromechanics*, 4(1):69–98, 2021. doi: 10.1504/IJHM.2021.114174. URL <https://www.inderscienceonline.com/doi/abs/10.1504/IJHM.2021.114174>.
- Hardoon, D. R., Szedmak, S., and Shawe-Taylor, J. Canonical correlation analysis: An overview with application to learning methods. *Neural Computation*, 16(12):2639–2664, 2004. doi: 10.1162/0899766042321814.
- Hotelling, H. Relations between two sets of variates. *Biometrika*, 28(3/4):321, dec 1936. doi: 10.2307/2333955. URL <https://doi.org/10.2307%2F2333955>.
- Humble, R., O’Shea, F. H., Colocho, W., Gibbs, M., Chaffee, H., Darve, E., and Ratner, D. Beam-based rf station fault identification at the slac linac coherent light source. *Phys. Rev. Accel. Beams*, 25:122804, Dec 2022. doi: 10.1103/PhysRevAccelBeams.25.122804. URL <https://link.aps.org/doi/10.1103/PhysRevAccelBeams.25.122804>.
- Kingma, D. P. and Ba, J. Adam: A method for stochastic optimization. In Bengio, Y. and LeCun, Y. (eds.), *3rd International Conference on Learning Representations, ICLR 2015, San Diego, CA, USA, May 7-9, 2015, Conference Track Proceedings*, 2015. URL <http://arxiv.org/abs/1412.6980>.
- Lindemann, B., Maschler, B., Sahlab, N., and Weyrich, M. A survey on anomaly detection for technical systems using lstm networks. *Computers in Industry*, 131:103498, 2021. ISSN 0166-3615. doi: <https://doi.org/10.1016/j.compind.2021.103498>. URL <https://www.sciencedirect.com/science/article/pii/S0166361521001056>.
- Liu, F. T., Ting, K. M., and Zhou, Z.-H. Isolation forest. In *2008 Eighth IEEE International Conference on Data Mining*. IEEE, dec 2008. doi: 10.1109/icdm.2008.17. URL <https://doi.org/10.1109%2Ficdm.2008.17>.
- Luo, S., Yuan, W., Adelson, E., Cohn, A. G., and Fuentes, R. ViTac: Feature sharing between vision

- and tactile sensing for cloth texture recognition. In 2018 IEEE International Conference on Robotics and Automation (ICRA). IEEE, may 2018. doi: 10.1109/icra.2018.8460494. URL <https://doi.org/10.1109%2Ficra.2018.8460494>.
- Lutz, M.-A., Vogt, S., Berkhout, V., Faulstich, S., Di-
enst, S., Steinmetz, U., Gück, C., and Ortega, A. Eval-
uation of anomaly detection of an autoencoder based
on maintenace information and scada-data. Energies,
13(5):1063, Feb 2020. ISSN 1996-1073. doi: 10.
3390/en13051063. URL [http://dx.doi.org/10.
3390/en13051063](http://dx.doi.org/10.3390/en13051063).
- Parzen, E. On estimation of a probability density func-
tion and mode. The Annals of Mathematical Statistics,
33(3):1065–1076, sep 1962. doi: 10.1214/aoms/
1177704472. URL [https://doi.org/10.1214%
2Faoms%2F1177704472](https://doi.org/10.1214%2Faoms%2F1177704472).
- Paszke, A., Gross, S., Massa, F., Lerer, A., Bradbury, J.,
Chanan, G., Killeen, T., Lin, Z., Gimelshein, N., Antiga,
L., Desmaison, A., Kopf, A., Yang, E., DeVito, Z.,
Raison, M., Tejani, A., Chilamkurthy, S., Steiner, B.,
Fang, L., Bai, J., and Chintala, S. Pytorch: An imperative
style, high-performance deep learning library. In Wallach,
H., Larochelle, H., Beygelzimer, A., d'Alché-Buc, F.,
Fox, E., and Garnett, R. (eds.), Advances in Neural
Information Processing Systems, volume 32. Curran As-
sociates, Inc., 2019. URL [https://proceedings.
neurips.cc/paper/2019/file/
bdbca288fee7f92f2bfa9f7012727740-Paper.
pdf](https://proceedings.neurips.cc/paper/2019/file/bdbca288fee7f92f2bfa9f7012727740-Paper.pdf).
- Radaideh, M., Pappas, C., Ramuhalli, P., and Cousineau,
S. Application of convolutional and feedforward neu-
ral networks for fault detection in particle accelera-
tor power systems. Annual Conference of the PHM
Society, 14(1), oct 2022. doi: 10.36001/phmconf.2022.
v14i1.3270. URL [https://doi.org/10.36001%
2Fphmconf.2022.v14i1.3270](https://doi.org/10.36001%2Fphmconf.2022.v14i1.3270).
- Ruff, L., Vandermeulen, R., Goernitz, N., Deecke, L.,
Siddiqui, S. A., Binder, A., Müller, E., and Kloft, M.
Deep one-class classification. In Dy, J. and Krause, A.
(eds.), Proceedings of the 35th International Conference
on Machine Learning, volume 80 of Proceedings of
Machine Learning Research, pp. 4393–4402. PMLR, 10–
15 Jul 2018. URL [https://proceedings.mlr.
press/v80/ruff18a.html](https://proceedings.mlr.press/v80/ruff18a.html).
- Schlegl, T., Seeböck, P., Waldstein, S. M., Schmidt-Erfurth,
U., and Langs, G. Unsupervised anomaly detection
with generative adversarial networks to guide marker
discovery. In Lecture Notes in Computer Science, pp.
146–157. Springer International Publishing, 2017. doi:
10.1007/978-3-319-59050-9_12. URL [https://doi.
org/10.1007%2F978-3-319-59050-9_12](https://doi.org/10.1007%2F978-3-319-59050-9_12).
- Schölkopf, B., Platt, J. C., Shawe-Taylor, J., Smola,
A. J., and Williamson, R. C. Estimating the sup-
port of a high-dimensional distribution. Neural
Computation, 13(7):1443–1471, jul 2001. doi: 10.1162/
089976601750264965. URL [https://doi.org/10.
1162%2F089976601750264965](https://doi.org/10.1162%2F089976601750264965).
- Storch, H. v. and Zwiers, F. W. Statistical Analysis in
Climate Research. Cambridge University Press, 1999.
doi: 10.1017/CBO9780511612336.
- Sun, W., Shao, S., Zhao, R., Yan, R., Zhang, X., and Chen,
X. A sparse auto-encoder-based deep neural network
approach for induction motor faults classification. Measurement,
89:171–178, 2016. ISSN 0263-2241.
doi: <https://doi.org/10.1016/j.measurement.2016.04.007>.
URL [https://www.sciencedirect.com/
science/article/pii/S0263224116300641](https://www.sciencedirect.com/science/article/pii/S0263224116300641).
- van der Maaten, L. and Hinton, G. Visualizing data using t-
sne. Journal of Machine Learning Research, 9(86):2579–
2605, 2008. URL [http://jmlr.org/papers/v9/
vandermaaten08a.html](http://jmlr.org/papers/v9/vandermaaten08a.html).
- Wallace, J. M., Smith, C., and Bretherton, C. S. Singu-
lar value decomposition of wintertime sea
surface temperature and 500-mb height anoma-
lies. Journal of Climate, 5(6):561–576, jun
1992. doi: 10.1175/1520-0442(1992)005<0561:
svdows>2.0.co;2. URL [https://doi.org/10.
1175%2F1520-0442%281992%29005%3C0561%
3Asvdows%3E2.0.co%3B2](https://doi.org/10.1175%2F1520-0442%281992%29005%3C0561%3Asvdows%3E2.0.co%3B2).
- Wang, W., Arora, R., Livescu, K., and Bilmes, J.
On deep multi-view representation learning. In
Proceedings of the 32nd International Conference on
International Conference on Machine Learning - Volume
37, ICML'15, pp. 1083–1092. JMLR.org, 2015.
- Zhao, R., Yan, R., Chen, Z., Mao, K., Wang, P., and
Gao, R. X. Deep learning and its applications to
machine health monitoring. Mechanical Systems and
Signal Processing, 115:213–237, 2019. ISSN 0888-
3270. doi: [https://doi.org/10.1016/j.ymssp.2018.05.
050](https://doi.org/10.1016/j.ymssp.2018.05.050). URL [https://www.sciencedirect.com/
science/article/pii/S0888327018303108](https://www.sciencedirect.com/science/article/pii/S0888327018303108).

A. Supplementary Materials for Section 2 (Coincident Learning)

A.1. CoAD Objective (Proofs)

Theorem 2.1. Assume that s and q are independent conditioned on knowing the true label, and assume that the algorithms $A_{\theta_s}, A_{\theta_q}$ are no worse than random guessers. Define $D(\theta_s, \theta_q) = \mathbb{E}_{(s,q) \in \mathcal{D}} [p_s | \neg p_q] \mathbb{E}_{(s,q) \in \mathcal{D}} [p_q | \neg p_s]$ to be our estimated fraction of false positives. Then, in the categorical case, the fraction of false positives is no more than D and the fraction of true positives is at least $J - D$, implying that \hat{R}, \hat{P} , and \hat{F}_β are lower bounds of their supervised counterparts R, P , and F_β .

Proof. Let $y(s, q)$ denote the true label (0-normal, 1-anomalous). For categorical $p_s(s), p_q(q)$, the fraction of false positives is

$$\mathbb{E}_{\mathcal{D}} [p_s p_q \neg y] = \mathbb{E} [p_s | \neg y] \mathbb{E} [p_q | \neg y] \mathbb{P}(\neg y)$$

where we use the independence of s and q conditioned on the true label. Since we do not have the labels, we cannot directly measure $\mathbb{E} [p_s | \neg y]$ and $\mathbb{E} [p_q | \neg y]$. We instead will bound this expectation:

$$\begin{aligned} \mathbb{E} [p_s | \neg y] &= \mathbb{P}(p_s | \neg y) = \mathbb{P}(p_s | p_q, \neg y) \\ &= \mathbb{P}(p_s | \neg p_q) - (\mathbb{P}(p_s | y) - \mathbb{P}(p_s | \neg y)) \mathbb{P}(y | \neg p_q) \\ &\leq \mathbb{P}(p_s | \neg p_q) = \mathbb{E} [p_s | \neg p_q] \end{aligned}$$

where in the first line we use the independence of s and q within a single class of data, and in the final line we use $\mathbb{P}(p_s | y) \geq \mathbb{P}(p_s | \neg y)$ (i.e., the algorithm is no worse than random). In the second line we use the identity

$$\begin{aligned} \mathbb{P}(p_s | \neg p_q) &= \mathbb{P}(p_s | \neg p_q, \neg y) \mathbb{P}(\neg y | \neg p_q) + \mathbb{P}(p_s | \neg p_q, y) \mathbb{P}(y | \neg p_q) \\ &= \mathbb{P}(p_s | \neg p_q, \neg y) (1 - \mathbb{P}(y | \neg p_q)) + \mathbb{P}(p_s | \neg p_q, y) \mathbb{P}(y | \neg p_q) \\ &= \mathbb{P}(p_s | \neg p_q, \neg y) - (\mathbb{P}(p_s | \neg p_q, y) - \mathbb{P}(p_s | \neg p_q, \neg y)) \mathbb{P}(y | \neg p_q) \\ &= \mathbb{P}(p_s | \neg p_q, \neg y) - [\mathbb{P}(p_s | y) - \mathbb{P}(p_s | \neg y)] \mathbb{P}(y | \neg p_q) \end{aligned}$$

where we have again applied independence of s and q within a single class. Finally plugging in $\mathbb{E} [p_s | \neg y] \leq \mathbb{E} [p_s | \neg p_q]$, $\mathbb{E} [p_q | \neg y] \leq \mathbb{E} [p_q | \neg p_s]$ (by the same logic), and $\mathbb{P}(\neg y) \leq 1$, we find

$$\mathbb{E}_{\mathcal{D}} [p_s p_q \neg y] \leq \mathbb{E} [p_s | \neg p_q] \mathbb{E} [p_q | \neg p_s] = D(\theta_s, \theta_q)$$

Lastly, since $\mathbb{E}_{\mathcal{D}} [p_s p_q \neg y] \leq D(\theta_s, \theta_q)$, the fraction of true positives is

$$\begin{aligned} \mathbb{E}_{\mathcal{D}} [p_s p_q y] &= \mathbb{E}_{\mathcal{D}} [p_s p_q] - \mathbb{E}_{\mathcal{D}} [p_s p_q \neg y] \\ &\geq J(\theta_s, \theta_q) - D(\theta_s, \theta_q) \end{aligned}$$

and therefore $\hat{F}_\beta \leq F_\beta$. □

Corollary 2.2. Additionally define $D_{naive}(\theta_s, \theta_q) = \mathbb{E}_{s \in \mathcal{D}_s} [p_s] \mathbb{E}_{q \in \mathcal{D}_q} [p_q]$, which is equivalent to an assumption that s and q are completely independent. Then, $D(\theta_s, \theta_q) \leq D_{naive}$.

Proof. We have

$$\begin{aligned} \mathbb{E}_{\mathcal{D}} [p_s] &= \mathbb{E} [p_s | p_q] \mathbb{P}(p_q) + \mathbb{E} [p_s | \neg p_q] \mathbb{P}(\neg p_q) \\ &= \mathbb{E} [p_s | \neg p_q] + \mathbb{P}(p_q) (\mathbb{E} [p_s | p_q] - \mathbb{E} [p_s | \neg p_q]) \\ &\geq \mathbb{E} [p_s | \neg p_q] \end{aligned}$$

since $\mathbb{E} [p_s | p_q] \geq \mathbb{E} [p_s | \neg p_q]$ if the algorithms are no worse than random. □

A.2. Properties of CoAD (Proofs)

Theorem 2.3. Assume θ_s is fixed (with $\mu_s \in (0, 0.5]$). Let $w(q) = \mathbb{E}_{s|q \in \mathcal{D}_{s|q}}[p_s(s)]$. Then, the maximum of \hat{F}_β can be achieved by a (nearly) categorical solution: $p_q^*(q) = \mathbf{1}\{w(q) > \tau\} + \rho \mathbf{1}\{w(q) = \tau\}$ for some $\rho, \tau \in [0, 1]$.

Proof. We can directly optimize as follows

$$\begin{aligned}
 \max_{\substack{p_q \in [0,1]^n \\ \mu_q \in [0,0.5]}} \hat{F}_\beta &= (1 + \beta^2) \max_{\substack{p_q \in [0,1]^n \\ \mu_q \in [0,0.5]}} \frac{\mu_{sq} - \mu_s \mu_q}{\mu_{sq} + \beta^2 \alpha} \frac{1 - \mu_{sq}}{(1 - \mu_s)(1 - \mu_q)} \\
 &= \frac{1 + \beta^2}{1 - \mu_s} \left(\max_{\substack{p_q \in [0,1]^n \\ \mu_q \in [0,0.5]}} \frac{\mu_{sq} - \mu_s \mu_q}{\mu_{sq} + \beta^2 \alpha} \frac{1 - \mu_{sq}}{1 - \mu_q} \right) \\
 &= \frac{1 + \beta^2}{1 - \mu_s} \left[\max_{\gamma \in [0,0.5]} \left(\max_{\substack{p_q \in [0,1]^n \\ \mu_q = \gamma}} \frac{\mu_{sq} - \mu_s \gamma}{\mu_{sq} + \beta^2 \alpha} (1 - \mu_{sq}) \right) \frac{1}{1 - \gamma} \right] \\
 &= \frac{1 + \beta^2}{1 - \mu_s} \left[\max_{\gamma \in [0,0.5]} \frac{\mu_{sq}^*(\gamma) - \mu_s \gamma}{\mu_{sq}^*(\gamma) + \beta^2 \alpha} \frac{1 - \mu_{sq}^*(\gamma)}{1 - \gamma} \right]
 \end{aligned}$$

where $\mu_{sq}^*(\gamma)$ is the solution to the inner problem. The solution to the unconstrained inner problem is

$$\begin{aligned}
 \tilde{\mu}_{sq}(\gamma) &= \arg \max_{p_q} \frac{\mu_{sq} - \mu_s \gamma}{\mu_{sq} + \beta^2 \alpha} (1 - \mu_{sq}) \\
 &= \sqrt{(1 + \alpha \beta^2)(\mu_s \gamma + \alpha \beta^2)} - \alpha \beta^2
 \end{aligned}$$

since

$$\frac{\partial}{\partial \mu_{sq}} \left(\frac{\mu_{sq} - \mu_s \gamma}{\mu_{sq} + \beta^2 \alpha} (1 - \mu_{sq}) \right) = \frac{(1 + \alpha \beta^2)(\mu_s \gamma + \alpha \beta^2)}{(\mu_{sq} + \alpha \beta^2)^2} - 1$$

and

$$\frac{\partial^2}{\partial \mu_{sq}^2} \left(\frac{\mu_{sq} - \mu_s \gamma}{\mu_{sq} + \beta^2 \alpha} (1 - \mu_{sq}) \right) = -2 \frac{(1 + \alpha \beta^2)(\mu_s \gamma + \alpha \beta^2)}{(\mu_{sq} + \alpha \beta^2)^3} \leq 0.$$

Now we will show that $\mu_{sq}^*(\gamma) \leq \tilde{\mu}_{sq}(\gamma)$. First, we have

$$\begin{aligned}
 \mu_{sq}^2 &= \mathbb{E}[p_s p_q]^2 \\
 &\leq \mathbb{E}[p_s^2] \mathbb{E}[p_q^2] \quad \text{by Cauchy-Schwartz} \\
 &\leq \mathbb{E}[p_s] \mathbb{E}[p_q] \quad \text{since } p_s, p_q \in [0, 1] \\
 &= \mu_s \gamma
 \end{aligned}$$

and

$$\mu_{sq} \leq \frac{1}{2} \leq \frac{1}{2}(1 + \mu_s \gamma) \quad \text{since } \mu_{sq} \leq \mu_q \leq \frac{1}{2}.$$

We can now bound $(\mu_{sq} + \alpha \beta^2)^2$:

$$\begin{aligned}
 (\mu_{sq} + \alpha \beta^2)^2 &= \mu_{sq}^2 + 2\mu_{sq} \alpha \beta^2 + (\alpha \beta^2)^2 \\
 &\leq \mu_s \gamma + (1 + \mu_s \gamma) \alpha \beta^2 + (\alpha \beta^2)^2 \\
 &= (1 + \alpha \beta^2)(\mu_s \gamma + \alpha \beta^2) \\
 &= \tilde{\mu}_{sq}(\gamma).
 \end{aligned}$$

Therefore, we have shown $\mu_{sq}^*(\gamma) \leq \tilde{\mu}_{sq}(\gamma)$, and thus the (constrained) inner optimization problem amounts to just maximizing μ_{sq} :

$$\begin{aligned}\mu_{sq}^*(\gamma) &= \arg \max_{\substack{p_q \in [0,1]^n \\ \mu_q = \gamma}} \mu_{sq} \\ &= \arg \max_{\substack{p_q \in [0,1]^n \\ \mu_q = \gamma}} \mathbb{E}_{q \in \mathcal{D}_q} \left[p_q(q) \mathbb{E}_{s|q \in \mathcal{D}_{s|q}} [p_s(s)] \right] \\ &= \arg \max_{\substack{p_q \in [0,1]^n \\ \mu_q = \gamma}} \mathbb{E}_{q \in \mathcal{D}_q} [p_q(q) w(q)].\end{aligned}$$

In order to maximize this, we first assign p_q^* mass to those q with largest $w(q)$ and then progressively to those with smaller $w(q)$. We therefore have

$$p_q^*(q) = \begin{cases} 1 & w(q) > \tau(\gamma) \\ \rho(\gamma) & w(q) = \tau(\gamma) \\ 0 & w(q) < \tau(\gamma) \end{cases}$$

where $\rho(\gamma), \tau(\gamma)$ are set to achieve $\mu_q = \gamma$. Specifically, let $f_{w(q)}(w) = \mathbb{P}(w(q) = w)$ and $\bar{F}_{w(q)}(w) = \mathbb{P}(w(q) > w)$. If $\exists \tau(\gamma)$ such that $\bar{F}_{w(q)}(\tau(\gamma)) = \gamma$, then $\rho(\gamma) = 0$. Otherwise, let $\tau(\gamma) = \inf\{w : \bar{F}_{w(q)}(w) \leq \gamma\}$. By definition, this implies that $f_{w(q)}(\tau(\gamma)) \geq \gamma - \bar{F}_{w(q)}(\tau(\gamma))$, so we can set $\rho(\gamma) = \frac{\gamma - \bar{F}_{w(q)}(\tau(\gamma))}{f_{w(q)}(\tau(\gamma))} \in [0, 1]$. Generally, we have

$$\begin{aligned}\tau(\gamma) &= \inf\{w : \bar{F}_{w(q)}(w) \leq \gamma\} \\ \rho(\gamma) &= \begin{cases} 0 & \text{if } \bar{F}_{w(q)}(\tau(\gamma)) = \gamma \\ \frac{\gamma - \bar{F}_{w(q)}(\tau(\gamma))}{f_{w(q)}(\tau(\gamma))} & \text{o.w.} \end{cases}\end{aligned}$$

□

Corollary A.1. Define $\mu_{sq}^*(\gamma) = \arg \max_{p_q \in [0,1]^n, \mu_q = \gamma} \mu_{sq}$. Then, $\mu_{sq}^*(\gamma)$ is continuous in γ and concave increasing.

Proof. From its definition in Theorem 2.3, the function $\mu_{sq}^*(\gamma)$ is increasing and continuous. Moreover, as γ increases, $\tau(\gamma)$ decreases. As a consequence, $\mu_{sq}^*(\gamma)$ is concave. □

Theorem 2.4. Additionally, a non-categorical solution (i.e., with $\rho \notin \{0, 1\}$) can only be uniquely optimal if the constraint $\mu_q \leq 0.5$ is tight.

Proof. Starting at the end of the proof of Theorem 2.3, we note that $\tau(\gamma)$ is the generalized inverse of the complementary cumulative distribution function $\bar{F}_{w(q)}(w)$. If a unique inverse exists, $\mu_{sq}^*(\gamma)$ is differentiable on $(0, 1)$; moreover, $\rho(\gamma) = 0$ for all γ , and we have a categorical solution for $p_q^*(q)$ achieving the maximum.

If instead a unique inverse does not exist, $\mu_{sq}^*(\gamma)$ can have piecewise linear segments, where each segment corresponds to a different $\tau(\gamma)$ threshold and the endpoints of each segment correspond to different categorical solutions. We need to revisit the outer problem (over γ) to establish the form of the solution. As shown in Theorem 2.3 and Corollary A.1, $\mu_{sq}^*(\gamma)$ is concave increasing and is piecewise linear (where each segment corresponds to a different $\tau(\gamma)$ threshold and the endpoints of each segment correspond to different categorical solutions). We also have that

$$\begin{aligned}\mu_s \gamma &= \mathbb{E}[p_s \gamma] \\ &\leq \max_{\substack{p_q \in [0,1]^n \\ \mu_q = \gamma}} \mathbb{E}[p_s p_q] = \mu_{sq}^*(\gamma) \\ &\leq \min \left(\mathbb{E}[p_s 1], \max_{\substack{p_q \in [0,1]^n \\ \mu_q = \gamma}} \mathbb{E}[1 p_q] \right) = \min(\mu_s, \gamma) \\ &\leq \frac{1}{2}\end{aligned}$$

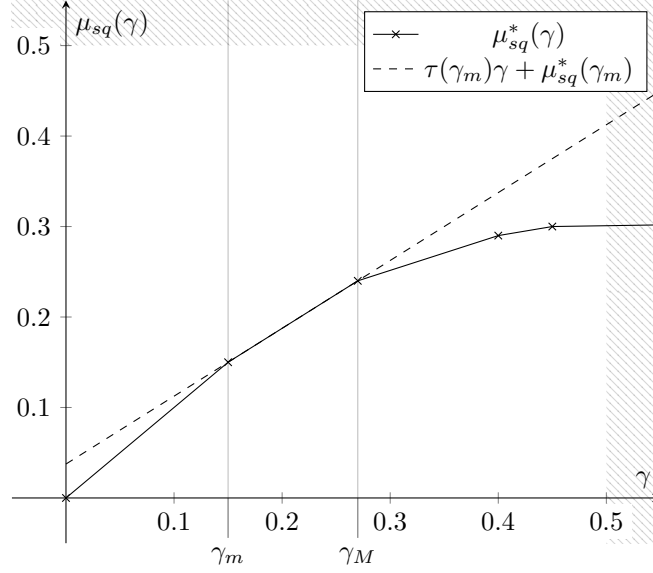


Figure 9. Illustration of piecewise linear behavior of $\mu_{sq}^*(\gamma)$.

and $0 \leq \tau(\gamma) \leq 1$.

We now consider where the maximum lies along each piecewise linear segment. Suppose there is a segment on $[\gamma_m, \gamma_M]$ with $0 \leq \gamma_m < \gamma_M \leq 0.5$. Along this segment, let $\mu_{sq}^*(\gamma) = ax + b$ where $a = \tau(\gamma_m)$, $b = \mu_{sq}^*(\gamma_m)$, and $x = \gamma - \gamma_m$. We depict this in Figure 9. The maximum along the segment is defined by

$$\begin{aligned} \arg \max_{\gamma \in [\gamma_m, \gamma_M]} \hat{F}_\beta(\gamma) &= \arg \max_{\gamma \in [\gamma_m, \gamma_M]} \frac{\mu_{sq}^*(\gamma) - \mu_s \gamma}{\mu_{sq}^*(\gamma) + \alpha \beta^2} \frac{1 - \mu_{sq}^*(\gamma)}{1 - \gamma} \\ &= \gamma_m + \arg \max_{x \in [0, \gamma_M - \gamma_m]} \frac{(b - \mu_s \gamma_m) + (a - \mu_s)x}{(b + \alpha \beta^2) + ax} \frac{(1 - b) - x}{(1 - \gamma_m) - x} \\ &= \gamma_m + \arg \max_{x \in [0, \gamma_M - \gamma_m]} f(x)g(x). \end{aligned}$$

Since $\mu_s \gamma \leq \mu_{sq}^*(\gamma) \leq \frac{1}{2}$, we immediately have $\hat{F}_\beta(\gamma) \geq 0$ for all $\gamma > 0$, which implies the null solution, $\gamma = 0$, is either not optimal or is not uniquely optimal, so we ignore it here-forward.

For $z = \alpha \beta^2(a - \mu_s) - \mu_s(b - a\gamma_m)$, we have

$$\begin{aligned} \frac{\partial}{\partial x} f(x) &= \frac{z}{((b + \alpha \beta^2) + ax)^2} \\ \frac{\partial^2}{\partial x^2} f(x) &= -\frac{2az}{((b + \alpha \beta^2) + ax)^3}. \end{aligned}$$

The denominators are positive, since they are non-negative and only 0 if $\alpha \beta^2 = \gamma_m = b = x = 0$ (which is the null solution). Therefore, $f(x)$ is (i) concave increasing if $z > 0$, (ii) constant if $z = 0$, or (iii) convex decreasing if $z < 0$. For $y = (1 - b) - a(1 - \gamma_m)$, we similarly have

$$\begin{aligned} \frac{\partial}{\partial x} g(x) &= \frac{y}{((1 - \gamma_m) - x)^2} \\ \frac{\partial^2}{\partial x^2} g(x) &= \frac{2y}{((1 - \gamma_m) - x)^3}. \end{aligned}$$

Since the denominators are positive, $g(x)$ is (i) convex increasing if $y > 0$, (ii) constant if $y = 0$, or (ii) concave decreasing

if $y < 0$. However $y \geq 0$:

$$\begin{aligned} y &= (1 - b) - a(1 - \gamma_m) \\ &= (1 - a) - (b - a\gamma_m) \\ &\geq 0 \end{aligned}$$

since $a = \tau(\gamma_m) \leq 1$ and $b = \mu_{sq}^*(\gamma_m) \geq \tau(\gamma_m)\gamma_m$ as $\mu_{sq}^*(\gamma_m)$ is concave increasing. We achieve $y = 0$ only if $a = 1, b = \gamma_m = 0$; if $y = 0$, we also have $z \geq 0$.

Therefore, there are only two scenarios to consider:

1. $z \geq 0$: $f(x)$ is constant or increasing, $g(x)$ is constant or increasing $\rightarrow \gamma^* = \gamma_M$
2. $z < 0$: $f(x)$ is convex decreasing, $g(x)$ is convex increasing. As we will show, $f(x)g(x)$ is convex $\rightarrow \gamma^* \in \{\gamma_m, \gamma_M\}$.

In the case that $z < 0$ (and $y > 0$ by the contrapositive), we have

$$\begin{aligned} \arg \max_{x \in [0, \gamma_M - \gamma_m]} f(x)g(x) &= \arg \max_{x \in [0, \gamma_M - \gamma_m]} \log(f(x)g(x)) \\ &= \arg \max_{x \in [0, \gamma_M - \gamma_m]} \log\left(\frac{(b - \mu_s \gamma_m) + (a - \mu_s)x}{(b + \alpha\beta^2) + ax} \frac{(1 - b) - ax}{(1 - \gamma_m) - x}\right) \\ &= \arg \max_{x \in [0, \gamma_M - \gamma_m]} \log\left(\frac{c_1 + c_2x}{c_3 + c_4x} \frac{c_5 - c_6x}{c_7 - x}\right) \end{aligned}$$

We consider the curvature of this:

$$\begin{aligned} \frac{\partial}{\partial x^2} \log\left(\frac{c_1 + c_2x}{c_3 + c_4x} \frac{c_5 - c_6x}{c_7 - x}\right) &= \left[\frac{c_4^2}{(c_3 + c_4x)^2} - \frac{c_2^2}{(c_1 + c_2x)^2}\right] + \left[\frac{1}{(c_7 - x)^2} - \frac{c_6^2}{(c_5 - c_6x)^2}\right] \\ &> 0 \text{ if } c_1c_4 > c_2c_3 \text{ and } c_5 > c_6c_7 \end{aligned}$$

But these conditions are equivalent to $z < 0$ and $g(x)$ increasing:

$$\begin{aligned} c_1c_4 - c_2c_3 &= a(b - \mu_s \gamma_m) - (a - \mu_s)(b + \alpha\beta^2) & c_5 - c_6c_7 &= 1 - b - a(1 - \gamma_m) \\ &= \mu_s(b - a\gamma_m) - \alpha\beta^2(a - \mu_s) & &= y > 0. \\ &= -z > 0 \end{aligned}$$

Since we are maximizing a convex function over a bounded domain, the maximizer is one of the domain endpoints, which implies the endpoints of all of the segments (except for possibly $\gamma_M = 0.5$) correspond to categorical solutions. Therefore, the only possible optimal non-categorical solution, where $\rho > 0$, occurs when the constraint $\mu_q \leq 0.5$ is tight. \square

Lemma A.2. Suppose two solutions with $\mu_{sq}^{(1)}, \mu_{sq}^{(2)}$ and $D^{(1)}, D^{(2)}$ respectively, where $D = \frac{\mu_s - \mu_{sq}}{1 - \mu_s} \frac{\mu_q - \mu_{sq}}{1 - \mu_q}$. Assume that $\mu_{sq}^{(1)} \geq D^{(1)}$ and $\mu_{sq}^{(2)} \geq D^{(2)}$. Wlog let $\mu_{sq}^{(1)} \geq \mu_{sq}^{(2)}$. Then, $\hat{F}_\beta^{(1)} > \hat{F}_\beta^{(2)}$ iff $z > 0, \beta^2 > \beta_{crit}^2$ where $z = \left(\mu_{sq}^{(1)} - \mu_{sq}^{(2)}\right) - (D^{(1)} - D^{(2)})$ and $\beta_{crit}^2 = \frac{\mu_{sq}^{(2)}D^{(1)} - \mu_{sq}^{(1)}D^{(2)}}{\alpha z}$. Moreover, $\hat{F}_\beta^{(1)} = \hat{F}_\beta^{(2)}$ iff $\mu_{sq}^{(1)} = \mu_{sq}^{(2)}, D^{(1)} = D^{(2)}$.

Proof. Using the alternate definition of \hat{F}_β , we see that $\hat{F}_\beta^{(1)} \geq \hat{F}_\beta^{(2)}$ iff

$$(1 + \beta^2) \frac{\mu_{sq}^{(1)} - D^{(1)}}{\mu_{sq}^{(1)} + \alpha\beta^2} \geq (1 + \beta^2) \frac{\mu_{sq}^{(2)} - D^{(2)}}{\mu_{sq}^{(2)} + \alpha\beta^2}.$$

This is equivalent to

$$\alpha\beta^2 \left(\mu_{sq}^{(1)} - \mu_{sq}^{(2)} + D^{(2)} - D^{(1)}\right) \geq \mu_{sq}^{(2)}D^{(1)} - \mu_{sq}^{(1)}D^{(2)}.$$

Let $z = \mu_{sq}^{(1)} - \mu_{sq}^{(2)} + D^{(2)} - D^{(1)}$, and $c = \mu_{sq}^{(2)} D^{(1)} - \mu_{sq}^{(1)} D^{(2)}$. We can also write $c = (\mu_{sq}^{(1)} - \mu_{sq}^{(2)}) (\mu_{sq}^{(1)} - D^{(1)}) - \mu_{sq}^{(1)} z$. The first term is always at least 0 by assumption. Therefore, if $z \leq 0$, we must have $c \geq 0$, and $\hat{F}_\beta^{(1)}$ is never strictly better; it is equal iff $z = 0, \mu_{sq}^{(1)} = \mu_{sq}^{(2)}$. $\hat{F}_\beta^{(1)}$ is strictly better iff $z > 0, \alpha\beta^2 > \frac{c}{z}$. \square

Theorem 2.5. *Suppose the variable x exists in some probability space $(\Omega, \mathcal{F}, \mathbb{P})$. As depicted in Figure 3, denote $A \in \mathcal{F}$ and A^c its complement, where $\alpha = \mathbb{P}(A) \leq 0.5$. Assume (i) $s(A) \cap s(A^c) = s(B)$ and $q(A) \cap q(A^c) = q(C)$; (ii) s and q are independent when $x \in A$ (and similarly when $x \in A^c$); (iii) $\mathbb{P}(A \cup B), \mathbb{P}(A \cup C) \leq 0.5$; (iv) $\mathbb{P}(A \setminus B \setminus C) > 0$; (v) $\mathbb{P}(A^c \setminus B \setminus C) \geq \mathbb{P}(A^c \setminus B)\mathbb{P}(A^c \setminus C)$; and (vi) $\mathbb{P}(A^c \setminus B \setminus C)\mathbb{P}(A \setminus C) \geq \mathbb{P}(A \setminus B \setminus C)\mathbb{P}(A^c \setminus C)$. Wlog let $\mathbb{P}(A \setminus B) \geq \mathbb{P}(A \setminus C)$. Then the maximum of \hat{F}_β is achieved when*

$$\begin{aligned} p_s(s(A \setminus B)) &\equiv 1, & p_q(q(A \setminus C)) &\equiv 1, \\ p_s(s(A^c \setminus B)) &\equiv 0, & p_q(q(A^c \setminus C)) &\equiv 0, \\ p_s(s(B)) &\equiv \mathbf{1}\{\beta^2 \geq \beta_{crit}^2\}, & p_q(q(C)) &\equiv 1. \end{aligned}$$

where β_{crit} depends on the sets A, A^c, B , and C .

Proof. Define

$$\begin{aligned} \mathbb{P}(A \setminus B \setminus C) &= c_1 \mathbb{P}(A) & \mathbb{P}(A^c \setminus B \setminus C) &= c_4 \mathbb{P}(A^c) \\ \mathbb{P}(A \setminus B) &= (c_1 + c_2) \mathbb{P}(A) & \mathbb{P}(A^c \setminus B) &= (c_4 + c_5) \mathbb{P}(A^c) \\ \mathbb{P}(A \setminus C) &= (c_1 + c_3) \mathbb{P}(A) & \mathbb{P}(A^c \setminus C) &= (c_4 + c_6) \mathbb{P}(A^c) \\ d_1 &= \frac{0.5 - \mathbb{P}(A \cup B)}{\mathbb{P}(A^c \setminus B)} & d_2 &= \frac{0.5 - \mathbb{P}(A \cup C)}{\mathbb{P}(A^c \setminus C)} \\ d_3 &= \frac{0.5}{\mathbb{P}(A^c \setminus B)} & d_4 &= \frac{0.5}{\mathbb{P}(A^c \setminus C)} \end{aligned}$$

At first glance, assigning the sets to labels looks combinatorially difficult, since it is unclear in what order we should assign labels to sets and if any set(s) should be always be labeled the same. We proceed by eliminating most possibilities. By Theorem 2.3 and Theorem 2.4, specifically the form of $p_q^*(q)$ (depending on $w(q) = \mathbb{E}_{s|q \in \mathcal{D}_{s|q}}[p_s(s)]$) and the (near) categorical optimal, we can determine which forms of the solution are possible.

Consider a fixed $p_s(s)$ assignment with $p_s(s(A \setminus B)) = v_1, p_s(s(B)) = v_2, p_s(s(A^c \setminus B)) = v_3$. The question is then in what order do we label $q(A \setminus C), q(C), q(A^c \setminus C)$. Using the independence of s and q within A and A^c (i.e., $\frac{c_1}{c_1 + c_3} = \frac{c_2}{1 - (c_1 + c_3)}$), we have

$$\begin{aligned} w(q(A \setminus C)) &= \frac{v_1 c_1 + v_2 c_3}{c_1 + c_3} = \frac{v_1 c_2 + v_2 (1 - (c_1 + c_2 + c_3))}{1 - (c_1 + c_3)} \\ w(q(A^c \setminus C)) &= \frac{v_3 c_4 + v_2 c_6}{c_4 + c_6} = \frac{v_3 c_5 + v_2 (1 - (c_4 + c_5 + c_6))}{1 - (c_4 + c_6)} \\ w(q(C)) &= \frac{(v_1 c_2 + v_2 (1 - c_1 - c_2 - c_3)) \mathbb{P}(A) + (v_3 c_5 + v_2 (1 - c_4 - c_5 - c_6)) \mathbb{P}(A^c)}{(1 - (c_1 + c_3)) \mathbb{P}(A) + (1 - (c_4 + c_6)) \mathbb{P}(A^c)}. \end{aligned}$$

Note that $w(q(C))$ is a particular combination of $w(q(A \setminus C))$ and $w(q(A^c \setminus C))$ such that either $w(q(A \setminus C)) \geq w(q(C)) \geq w(q(A^c \setminus C))$ or $w(q(A \setminus C)) \leq w(q(C)) \leq w(q(A^c \setminus C))$. Therefore, for any setting of v_1, v_2, v_3 , we will label in either the order $q(A \setminus C), q(C), q(A^c \setminus C)$ or $q(A^c \setminus C), q(C), q(A \setminus C)$.

By flipping the role of p_s and p_q and applying this logic again, we need only consider solutions in s and q that label in this manner. Moreover, s and q will label in the same order. Concretely, suppose we labeled s in the order $s(A \setminus B), s(B), s(A^c \setminus B)$, with one of the labeling possibilities respecting the constraint $\mu_s \leq 0.5$: (i) $v_1 = 1, v_2 = v_3 = 0$; (ii) $v_1 = v_2 = 1, v_3 = 0$; or (iii) $v_1 = v_2 = 1, v_3 = d_2$. Then, we also label q in the order $q(A \setminus C), q(C), q(A^c \setminus C)$ as $w(q(A \setminus C)) \geq w(q(A^c \setminus C))$ under each possibility.

As a result, there are only 8 possible optimal solutions, that can be split into 3 groups:

- $p_s(s(A \setminus B)) = p_q(q(A \setminus C)) = 1, p_s(s(B)) = \rho, p_q(q(C)) = \eta, p_s(s(A^c \setminus B)) = p_q(q(A^c \setminus C)) = 0$: Four possible solutions with $\rho^*, \eta^* \in \{0, 1\}$.
- $p_s(s(A \cup B)) = p_q(q(A \cup C)) = 1, p_s(s(A^c \setminus B)) = \rho, p_q(q(A^c \setminus C)) = \eta$: Three additional possible solutions with $(\rho^*, \eta^*) \in \{(0, d_2), (d_1, 0), (d_1, d_2)\}$.
- $p_s(s(A \cup B)) = p_q(q(A \cup C)) = 0, p_s(s(A^c \setminus B)) = \rho, p_q(q(A^c \setminus C)) = \eta$: One only possible solution $\rho^* = d_3, \eta^* = d_4$.

Let's consider the first group, with $p_s(s(A \setminus B)) = p_q(q(A \setminus C)) = 1, p_s(s(A^c \cup B)) = \rho, p_q(q(A^c \cup C)) = \eta, p_s(s(A^c \setminus B)) = p_q(q(A^c \setminus C)) = 0$. We have

$$\begin{aligned}\mu_{sq} &= [c_1 + \rho c_3 + \eta c_2 + \rho\eta(1 - c_1 - c_2 - c_3)] \mathbb{P}(A) + \rho\eta(1 - c_4 - c_5 - c_6) \mathbb{P}(A^c) \\ \mu_s &= [(c_1 + c_2) + \rho(1 - c_1 - c_2)] \mathbb{P}(A) + \rho(1 - c_4 - c_5) \mathbb{P}(A^c) \\ \mu_q &= [(c_1 + c_3) + \eta(1 - c_1 - c_3)] \mathbb{P}(A) + \eta(1 - c_4 - c_6) \mathbb{P}(A^c) \\ \frac{\mu_s - \mu_{sq}}{1 - \mu_s} &= \frac{(1 - \eta) [c_2 + \rho(1 - c_1 - c_2 - c_3)] \mathbb{P}(A) + \rho [(1 - \eta)(1 - c_4 - c_5) + \eta c_6] \mathbb{P}(A^c)}{(1 - \rho)(1 - c_1 - c_2) \mathbb{P}(A) + [1 - \rho(1 - c_4 - c_5)] \mathbb{P}(A^c)} \\ \frac{\mu_q - \mu_{sq}}{1 - \mu_q} &= \frac{(1 - \rho) [c_3 + \eta(1 - c_1 - c_2 - c_3)] \mathbb{P}(A) + \eta [(1 - \rho)(1 - c_4 - c_6) + \rho c_5] \mathbb{P}(A^c)}{(1 - \eta)(1 - c_1 - c_3) \mathbb{P}(A) + [1 - \eta(1 - c_4 - c_6)] \mathbb{P}(A^c)}\end{aligned}$$

Note that due to the assumption $\mathbb{P}(A \setminus B) \geq \mathbb{P}(A \setminus C)$, we have $c_2 \geq c_3 \geq 0$. To analyze the possible solutions $(\rho^*, \eta^* \in \{0, 1\})$, we consider the alternate definition for \hat{F}_β

$$\begin{aligned}\hat{F}_\beta &= (1 + \beta^2) \frac{\mu_{sq} - D}{\mu_{sq} + \alpha\beta^2} \\ D &= \frac{\mu_s - \mu_{sq}}{1 - \mu_q} \frac{\mu_q - \mu_{sq}}{1 - \mu_s}\end{aligned}$$

under the four options:

- $\rho^* = \eta^* = 0$: Since $\mu_s, \mu_q \geq \mu_{sq}$, we have $D \geq 0$ and

$$\hat{F}_\beta = (1 + \beta^2) \frac{c_1 \mathbb{P}(A) - D}{c_1 \mathbb{P}(A) + \alpha\beta^2}$$

- $\rho^* = 1, \eta^* = 0$: Since $\mu_{sq} = \mu_q$, we have $D = 0$ and

$$\hat{F}_\beta = (1 + \beta^2) \frac{(c_1 + c_3) \mathbb{P}(A)}{(c_1 + c_3) \mathbb{P}(A) + \alpha\beta^2}$$

- $\rho^* = 0, \eta^* = 1$: Since $\mu_{sq} = \mu_s$, we have $D = 0$ and

$$\hat{F}_\beta = (1 + \beta^2) \frac{(c_1 + c_2) \mathbb{P}(A)}{(c_1 + c_2) \mathbb{P}(A) + \alpha\beta^2}$$

- $\rho^* = \eta^* = 1$

$$\begin{aligned}\hat{F}_\beta &= (1 + \beta^2) \frac{\mathbb{P}(A) + (1 - c_4 - c_5 - c_6) \mathbb{P}(A^c) - D}{\mathbb{P}(A) + (1 - c_4 - c_5 - c_6) \mathbb{P}(A^c) + \alpha\beta^2} \\ D &= \frac{c_5}{c_4 + c_5} \frac{c_6}{c_4 + c_6}\end{aligned}$$

Since $D(\rho^* = 0, \eta^* = 0) \geq 0$, we have

$$\hat{F}_\beta(\rho^* = 1, \eta^* = 0) \geq \hat{F}_\beta(\rho^* = 0, \eta^* = 0)$$

where the inequality is equality iff $c_3 = 0$. Furthermore, since $c_2 \geq c_3 \geq 0$, we have

$$\hat{F}_\beta(\rho^* = 0, \eta^* = 1) \geq \hat{F}_\beta(\rho^* = 1, \eta^* = 0)$$

where the inequality is equality iff $\beta = 0$ or $c_2 = c_3$. The relationship between $\hat{F}_\beta(\rho^* = 0, \eta^* = 1)$ and $\hat{F}_\beta(\rho^* = 1, \eta^* = 1)$ depends on the various probabilities and also the setting of β . Specifically, by Lemma A.2, we have

$$\hat{F}_\beta(\rho^* = 1, \eta^* = 1) > \hat{F}_\beta(\rho^* = 0, \eta^* = 1)$$

iff $z > 0$ and $\beta^2 > \beta_{\text{crit}}^2$ where

$$\begin{aligned} z &= (\mu_{sq}(\rho^* = 1, \eta^* = 1) - \mu_{sq}(\rho^* = 0, \eta^* = 1)) - (D(\rho^* = 1, \eta^* = 1) - D(\rho^* = 0, \eta^* = 1)) \\ &= ((1 - c_1 - c_2)\mathbb{P}(A) + (1 - c_4 - c_5 - c_6)\mathbb{P}(A^c)) - \frac{c_5}{c_4 + c_5} \frac{c_6}{c_4 + c_6} \\ &= \mathbb{P}(A \cap B) + \mathbb{P}(A^c \cap B \cap C) - \frac{\mathbb{P}((A^c \setminus B) \cap C)}{\mathbb{P}(A^c \setminus B)} \frac{\mathbb{P}((A^c \setminus C) \cap B)}{\mathbb{P}(A^c \setminus C)} \\ \beta_{\text{crit}}^2 &= \frac{\mu_{sq}(\rho^* = 0, \eta^* = 1)D(\rho^* = 1, \eta^* = 1) - \mu_{sq}(\rho^* = 1, \eta^* = 1)D(\rho^* = 0, \eta^* = 1)}{\alpha z} \\ &= \frac{(c_1 + c_2)\mathbb{P}(A)}{\alpha z} \frac{c_5}{c_4 + c_5} \frac{c_6}{c_4 + c_6} \\ &= \frac{\mathbb{P}(A \setminus B)}{\mathbb{P}(A)} \frac{\mathbb{P}((A^c \setminus B) \cap C)}{\mathbb{P}(A^c \setminus B)} \frac{\mathbb{P}((A^c \setminus C) \cap B)}{\mathbb{P}(A^c \setminus C)} \frac{1}{z} \end{aligned}$$

We have equality iff $c_5 c_6 = 0$ (i.e., B or C is the empty set); but by assumption ($\mathbb{P}(A \setminus B) \geq \mathbb{P}(A \setminus C)$), this must be satisfied first by $B = \emptyset$. In this case, we don't care about the setting of ρ . So whenever we care to label $s(B)$, the condition on z is always met under the assumption $\mathbb{P}(A^c \setminus B \setminus C)\mathbb{P}(A \setminus C) \geq \mathbb{P}(A \setminus B \setminus C)\mathbb{P}(A^c \setminus C)$:

$$\begin{aligned} z &= \mathbb{P}(A \cap B) + \mathbb{P}(A^c \cap B \cap C) - \frac{\mathbb{P}((A^c \setminus B) \cap C)}{\mathbb{P}(A^c \setminus B)} \frac{\mathbb{P}((A^c \setminus C) \cap B)}{\mathbb{P}(A^c \setminus C)} \\ &= \mathbb{P}(A \cap B) + \mathbb{P}(A^c \cap B \cap C) - \frac{\mathbb{P}((A^c \setminus B) \cap C)}{\mathbb{P}(A^c \setminus B)} \frac{\mathbb{P}((A^c \setminus C) \cap B)}{\mathbb{P}(A^c \setminus C)} \\ &= \mathbb{P}(A \cap B) - (1 - \mathbb{P}(A^c)) \frac{\mathbb{P}((A^c \setminus B) \cap C)}{\mathbb{P}(A^c \setminus B)} \frac{\mathbb{P}((A^c \setminus C) \cap B)}{\mathbb{P}(A^c \setminus C)} \\ &= \mathbb{P}(A \cap B) - \mathbb{P}(A) \frac{\mathbb{P}((A^c \setminus B) \cap C)}{\mathbb{P}(A^c \setminus B)} \frac{\mathbb{P}((A^c \setminus C) \cap B)}{\mathbb{P}(A^c \setminus C)} \\ &= \mathbb{P}(A) \left[\left(1 - \frac{\mathbb{P}(A \setminus B \setminus C)}{\mathbb{P}(A \setminus C)}\right) - \left(1 - \frac{\mathbb{P}(A^c \setminus B \setminus C)}{\mathbb{P}(A^c \setminus B)}\right) \left(1 - \frac{\mathbb{P}(A^c \setminus B \setminus C)}{\mathbb{P}(A^c \setminus C)}\right) \right] \\ &= \mathbb{P}(A) \left[\frac{\mathbb{P}(A^c \setminus B \setminus C)}{\mathbb{P}(A^c \setminus C)} - \frac{\mathbb{P}(A \setminus B \setminus C)}{\mathbb{P}(A \setminus C)} + \left(1 - \frac{\mathbb{P}(A^c \setminus B \setminus C)}{\mathbb{P}(A^c \setminus C)}\right) \frac{\mathbb{P}(A^c \setminus B \setminus C)}{\mathbb{P}(A^c \setminus B)} \right] \\ &> 0 \end{aligned}$$

where we used the equalities

$$\begin{aligned} \frac{\mathbb{P}(A^c \cap B \cap C)}{\mathbb{P}(A^c \cap B)} &= \frac{\mathbb{P}((A^c \setminus B) \cap C)}{\mathbb{P}(A^c \setminus B)} \\ \frac{\mathbb{P}(A^c \cap B)}{\mathbb{P}(A^c)} &= \frac{\mathbb{P}((A^c \setminus C) \cap B)}{\mathbb{P}(A^c \setminus C)} \\ \frac{\mathbb{P}(A \cap B)}{\mathbb{P}(A)} &= \frac{\mathbb{P}((A \setminus C) \cap B)}{\mathbb{P}(A \setminus C)} \end{aligned}$$

since s and q are independent within A and A^c .

Now, let's consider the second group, with $p_s(s(A \cup B)) = p_q(q(A \cup C)) = 1, p_s(s(A^c \setminus B)) = \rho, p_q(q(A^c \setminus C)) = \eta$. We can write

$$\begin{aligned}\mu_{sq} &= \mathbb{P}(A) + [(1 - c_4 - c_5 - c_6) + \rho c_5 + \eta c_6 + \rho \eta c_4] \mathbb{P}(A^c) \\ \mu_s &= \mathbb{P}(A) + [(1 - c_4 - c_5) + \rho(c_4 + c_5)] \mathbb{P}(A^c) \\ \mu_q &= \mathbb{P}(A) + [(1 - c_4 - c_6) + \eta(c_4 + c_6)] \mathbb{P}(A^c) \\ D &= \frac{c_6 + \rho c_4}{c_4 + c_6} \frac{c_5 + \eta c_4}{c_4 + c_5}\end{aligned}$$

We again analyze the possible solutions $((\rho^*, \eta^*) \in \{(0, d_2), (d_1, 0), (d_1, d_2)\})$, and compare to $(\rho^* = \eta^* = 0)$ for improvement:

- $\rho^* = 0, \eta^* = d_2$: By Lemma A.2 (the condition on z), this solution cannot be an improvement if

$$\begin{aligned}\mu_{sq}^*(\rho^* = 0, \eta^* = d_2) - \mu_{sq}^*(\rho^* = 0, \eta^* = 0) &\leq D(\rho^* = 0, \eta^* = d_2) - D(\rho^* = 0, \eta^* = 0) \\ d_2 c_6 \mathbb{P}(A^c) &\leq d_2 c_6 \frac{1}{c_4 + c_6} \frac{c_4}{c_4 + c_5} \\ \mathbb{P}(A^c) &\leq \frac{1}{c_4 + c_6} \frac{c_4}{c_4 + c_5},\end{aligned}$$

which is equivalently $\mathbb{P}(A^c \setminus B \setminus C) \geq \mathbb{P}(A^c \setminus B) \mathbb{P}(A^c \setminus C)$. This holds by assumption. The solutions are equal iff $c_6 = 0$.

- $\rho^* = d_1, \eta^* = 0$: By symmetry, this is not an improvement. The solutions are equal iff $c_5 = 0$.
- $\rho^* = d_1, \eta^* = d_2$: In fact, the same condition guarantees that this solution cannot be an improvement either, as we again have

$$\begin{aligned}\mu_{sq}^*(\rho^* = d_1, \eta^* = d_2) - \mu_{sq}^*(\rho^* = 0, \eta^* = 0) &\leq D(\rho^* = 0, \eta^* = d_2) - D(\rho^* = 0, \eta^* = 0) \\ [d_1 c_5 + d_2 c_6 + d_1 d_2 c_4] \mathbb{P}(A^c) &\leq [d_1 c_5 + d_2 c_6 + d_1 d_2 c_4] \frac{c_4}{(c_4 + c_6)(c_4 + c_5)} \\ \mathbb{P}(A^c) &\leq c_4 \frac{c_4}{(c_4 + c_6)(c_4 + c_5)}\end{aligned}$$

None of these solutions are improvements (or even equal except under corner cases) and therefore can be ignored.

Finally, let's consider the third group, with just the one possible solution: $p_s(s(A \cup B)) = p_q(q(A \cup C)) = 0, p_s(s(A^c \setminus B)) = d_3, p_q(q(A^c \setminus C)) = d_4$. We will compare this to $p_s(s(A \cup B)) = p_q(q(A \cup C)) = 1, p_s(s(A^c \setminus B)) = d_1, p_q(q(A^c \setminus C)) = d_2$. We can in fact we can show that the μ_{sq} for both solutions are equal: $d_3 d_4 c_4 \mathbb{P}(A^c) = \mathbb{P}(A) + [(1 - c_4 - c_5 - c_6) + d_1 c_5 + d_2 c_6 + d_1 d_2 c_4] \mathbb{P}(A^c)$ since $1 - d_1 = d_3, 1 - d_2 = d_4$. Moreover, since both solutions achieve $\mu_s = \mu_q = 0.5$, they are equal for all β . But since the solution we are comparing against is never optimal, this is never optimal either! \square

Theorem 2.6. Suppose p_s, p_q are parameterized as DNNs, whose final components of each DNN are a fully-connected layer and a sigmoid activation. Let the latent representation fed into the final layer be $z_s(s), z_q(q) \in \mathbb{R}^p$ for the two networks respectively. Define $p_s(s) = \sigma(w_s^T z_s(s) + b_s)$ and $p_q(q) = \sigma(w_q^T z_q(q) + b_q)$. Then,

$$\begin{aligned}\nabla_{w_s} \hat{F}_\beta &\equiv \mathbb{E}_{\mathcal{D}} [\hat{y}_q(q) \gamma_s(s) z_s(s)] \\ \nabla_{b_s} \hat{F}_\beta &\equiv \mathbb{E}_{\mathcal{D}} [\hat{y}_q(q) \gamma_s(s)] \\ \nabla_{z_s(s)} \hat{F}_\beta &\equiv \mathbb{E}_{\mathcal{D}_{q|s}} [\hat{y}_q(q) \gamma_s(s) z_s(s)]\end{aligned}$$

where $\hat{y}_p(p) = c_1 p_q(q) - c_2$ and $\gamma_s(s) = p_s(s) (1 - p_s(s))$. The gradients w.r.t. the q network are analogous. The constants c_1, c_2 depend on the current parameters θ_s, θ_q but not individual instances $(s, q) \in \mathcal{D}$. If the networks are better than random guessers, then $c_1, c_2 \geq 0$.

Proof. Recall that for $y = \sigma(a^T x + b)$, we have $\nabla_a y = y(1-y)x$ and $\nabla_b y = y(1-y)$. Let us consider the gradients w.r.t. the parameters of the linear classifier:

$$\begin{aligned}
 \nabla_{w_s} \hat{F}_\beta &= \nabla_{w_s} \left((1 + \beta^2) \frac{\mu_{sq} - \mu_s \mu_q}{\mu_{sq} + \alpha \beta^2} \frac{1 - \mu_{sq}}{(1 - \mu_s)(1 - \mu_q)} \right) \\
 &= \hat{F}_\beta \left[\frac{\nabla_{w_s}(1 - \mu_{sq})}{1 - \mu_{sq}} + \frac{\nabla_{w_s}(\mu_{sq} - \mu_s \mu_q)}{\mu_{sq} - \mu_s \mu_q} \right] \\
 &\quad - \hat{F}_\beta \left[\frac{\nabla_{w_s}(\mu_{sq} + \alpha \beta^2)}{\mu_{sq} + \alpha \beta^2} + \frac{\nabla_{w_s}(1 - \mu_s)}{1 - \mu_s} \right] \\
 &= \hat{F}_\beta \left[\frac{1}{\mu_{sq} - \mu_s \mu_q} - \frac{1}{1 - \mu_{sq}} - \frac{1}{\mu_{sq} + \alpha \beta^2} \right] \mathbb{E}_{\mathcal{D}}[p_q(q) \nabla_{w_s} p_s(s)] \\
 &\quad - \hat{F}_\beta \left[\frac{\mu_q}{\mu_{sq} - \mu_s \mu_q} - \frac{1}{1 - \mu_s} \right] \mathbb{E}_{\mathcal{D}}[\nabla_{w_s} p_s(s)] \\
 &= \mathbb{E}_{\mathcal{D}}[(c_1 p_q(q) - c_2) \nabla_{w_s} p_s(s)] \\
 &= \mathbb{E}_{\mathcal{D}}[(c_1 p_q(q) - c_2) p_s(s) (1 - p_s(s)) \nabla_{w_s} (w_s^T z_s(s) + b_s)] \\
 &\equiv \mathbb{E}_{\mathcal{D}}[\hat{y}_q(q) \gamma_s(s) z_s(s)]
 \end{aligned}$$

where we use the dominating convergence theorem to exchange the derivative and expectation (note that the expectations are finite and μ_{sq}, μ_s are differentiable for all choices of weights; moreover the derivatives are bounded). We have defined

$$\begin{aligned}
 \gamma_s(s) &= p_s(s)(1 - p_s(s)) \\
 \hat{y}_p(p) &= c_1 p_q(q) - c_2 \\
 c_1 &= \hat{F}_\beta \left[\frac{1}{\mu_{sq} - \mu_s \mu_q} - \frac{1}{1 - \mu_{sq}} - \frac{1}{\mu_{sq} + \alpha \beta^2} \right] \\
 c_2 &= \hat{F}_\beta \left[\frac{\mu_q}{\mu_{sq} - \mu_s \mu_q} - \frac{1}{1 - \mu_s} \right] \\
 &= \hat{F}_\beta \frac{\mu_q - \mu_{sq}}{(\mu_{sq} - \mu_s \mu_q)(1 - \mu_s)}
 \end{aligned}$$

The gradients w.r.t. the latent representation $z_s(s)$ under the \hat{F}_β loss is

$$\begin{aligned}
 \nabla_{z_s(s)} \hat{F}_\beta &= \mathbb{E}_{\mathcal{D}_{q|s}}[(c_1 p_q(q) - c_2) p_s(s) (1 - p_s(s))] \\
 &\equiv \mathbb{E}_{\mathcal{D}_{q|s}}[\hat{y}_q(q) \gamma_s(s) z_s(s)]
 \end{aligned}$$

Lastly, we can show that $c_1, c_2 \geq 0$ under the assumption that if the networks are better than random guessers (i.e., $\mu_{sq} \geq \mu_s \mu_q$). We have that $c_1 \geq 0$:

$$\begin{aligned}
 c_1 &= \hat{F}_\beta \left[\frac{1}{\mu_{sq} - \mu_s \mu_q} - \frac{1}{1 - \mu_{sq}} - \frac{1}{\mu_{sq} + \alpha \beta^2} \right] \\
 &= \hat{F}_\beta \left[\frac{-(\mu_{sq} - \mu_s \mu_q)(1 - \mu_{sq}) + (\mu_{sq} + \alpha \beta^2)(1 - 2\mu_{sq} + \mu_s \mu_q)}{(\mu_{sq} - \mu_s \mu_q)(1 - \mu_{sq})(\mu_{sq} + \alpha \beta^2)} \right] \\
 &= \hat{F}_\beta \left[\frac{(\mu_s \mu_q - \mu_{sq}^2) + \alpha \beta^2 (1 - 2\mu_{sq} + \mu_s \mu_q)}{(\mu_{sq} - \mu_s \mu_q)(1 - \mu_{sq})(\mu_{sq} + \alpha \beta^2)} \right] \\
 &\geq 0
 \end{aligned}$$

where $\mu_s \mu_q \geq \mu_{sq}^2$ by Cauchy-Schwartz (shown in more detail in the proof of Theorem 2.3) and since $\mu_{sq} \leq 0.5$. Also, since $\mu_{sq} \leq \mu_q$ by definition, we have $c_2 \geq 0$. \square

B. Supplementary Materials for Section 4 (Experiments)

In the continuous setting, where the algorithms are represented by DNNs, we need to enforce the constraints $\mu_s, \mu_q \leq 0.5$. In order to use gradient-based optimizers, we impose these constraints using a ‘‘wall’’ regularization term $\mathcal{L}_{\text{wall}} =$

$\mu_s \sigma(t(\mu_s - 0.5)) + \mu_q \sigma(t(\mu_q - 0.5))$ where t is the wall’s temperature (set to 50 for all experiments) and $\sigma(\cdot)$ is the sigmoid function. Also, to prevent the network from quickly railing to $\{0, 1\}$ (and thereby suffer from vanishing gradients), we impose a norm penalty on the magnitude of the output logits (i.e., outputs prior to the final sigmoid converting to probability): $\mathcal{L}_{\text{mag}} = \mathbb{E}[\text{logit}(p_s)^2 + \text{logit}(p_q)^2]$. In total, we minimize the loss

$$\mathcal{L} = -\hat{F}_\beta + \lambda_{\text{wall}} \mathcal{L}_{\text{wall}} + \lambda_{\text{mag}} \mathcal{L}_{\text{mag}}$$

where $\lambda_{\text{wall}}, \lambda_{\text{mag}}$ are the regularization strengths.

B.1. MNIST

For the MNIST example, we use a noisy observation model to ensure that each anomaly class (digits 1, 2 and 3) has a different amount of noise. In particular, we suppose that each anomaly digit has a weight w_i and a “blur” probability b_i . Then, for each stream of data independently, we replace the anomalous digit with the normal digit (i.e., 0) with probability b_i ; we also symmetrically replace the normal digit with the anomalous digit i with probability b_i . This creates a data set with mixed image pairs. For our experiments, we used the setting $w_0 = 0.85, w_1 = w_2 = w_3 = 0.05$ and $b_1 = 0, b_2 = 0.05, b_3 = 0.2$. It is worth noting that our experiment is not specific to this particular observation model: other ways of generating mixed image pairs would also work.

To better understand the behavior of our metric in this setting, we plot \hat{F}_β under the simplification that all digits of the same class are identical. This allows us to derive a closed form for \hat{F}_β as a function of the w_i, b_i, β , and the labeling choice $p_s(\text{digit } i) = p_q(\text{digit } i) = y_i$. We show the 3 obvious labeling choices in Figure 10. Each labeling choice is optimal for a range of β , and the higher choices of β (i.e., higher recall preference) lead to labeling the noisy classes as anomalous.

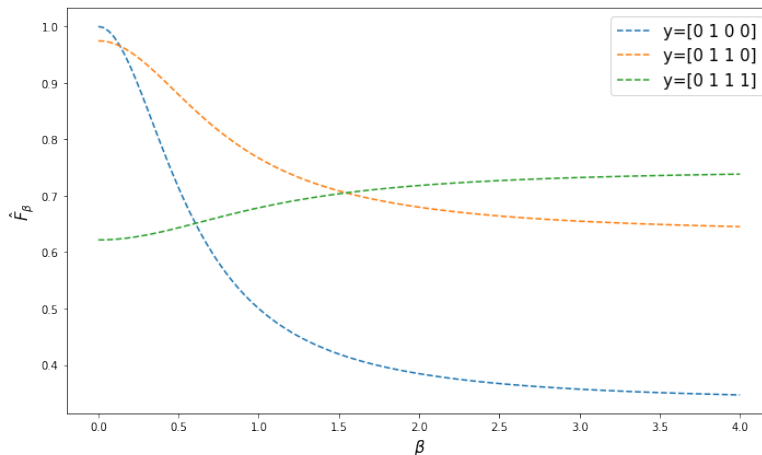


Figure 10. \hat{F}_β for different labeling choices and values of β , under the simplified MNIST model.

We transform each MNIST by randomly cropping it to 25×25 and rolling between 0 and 5 pixels along each dimension independently. We define our algorithms $A_{\theta_s}, A_{\theta_q}$ as convolutional neural networks (CNNs). As shown in Figure 11, our networks consist of four 2D convolutions with 10 out channels, kernel size 5, padding 2, and strides 1, 1, 2, 2 respectively, followed by three FC layers of output size 8, 8, 1 respectively. All layers but the final layer are followed by a ReLU activation. We train for 3000 epochs of 1800 image pairs, with a batch size of 760, and test by simultaneously feeding images to each network. We use the Adam optimizer (Paszke et al., 2019) with a learning rate of 10^{-4} . We set $\alpha = 0.15, \lambda_{\text{wall}} = 1/\alpha$, and $\lambda_{\text{mag}} = 0$.

For completeness, Figure 12 shows the violin plots corresponding to the results in Table 1.

B.2. Milling dataset

We define our algorithms $A_{\theta_s}, A_{\theta_q}$ as CNNs. As shown in Figure 13, our networks consist of two 1D convolutions with 10 out channels, kernel size 5, padding 2, and stride 1, followed by three FC layers of output size 8, 8, 1 respectively. All layers

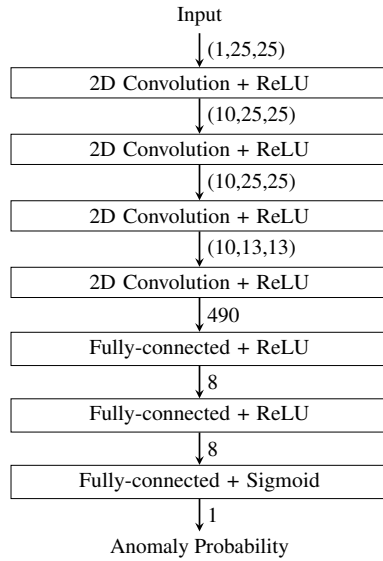


Figure 11. Model architecture for each MNIST DNN, showing the input size to each layer.

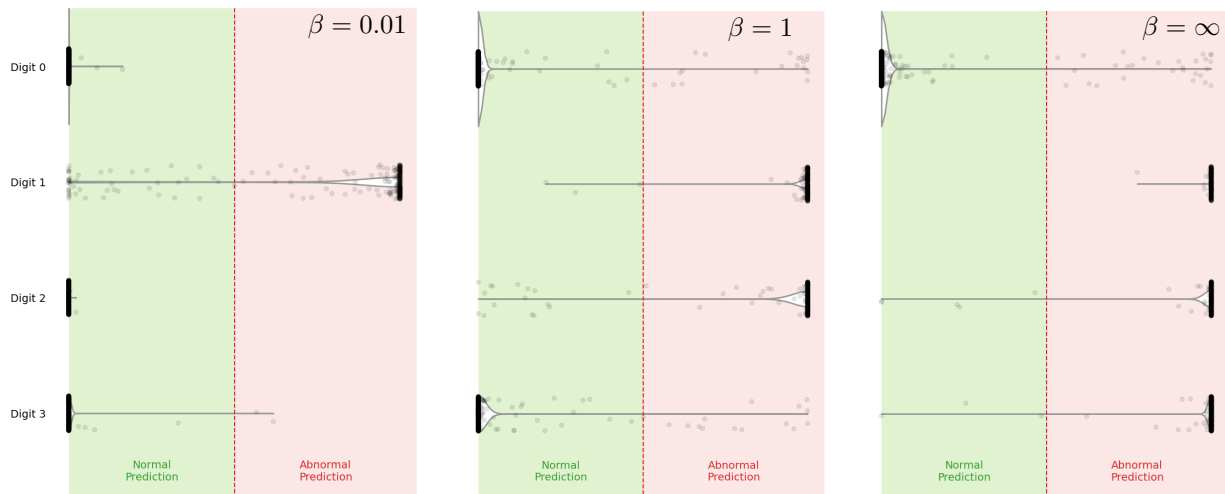


Figure 12. Violin plot showing predictions from the \hat{F}_β models on the MNIST digits. Prediction values are the products of the two network outputs. From left to right, $\beta = 0.01, 1, \infty$.

but the final layer are followed by a ReLU activation. The s net has 2 input channels; the q net has 4 input channels. We train for 50 epochs using a batch size of 1024 and the train-test splits of (Hahn & Mechefske, 2021). We use the Adam optimizer (Paszke et al., 2019) with a learning rate of 3×10^{-3} . We set $\alpha = 0.438$, according the flank wear labels. We set $\lambda_{\text{wall}} = 1$ and $\lambda_{\text{mag}} = 2e - 4$.

As discussed in Section 4.3, the labels defined in (Hahn & Mechefske, 2021) are quite simplistic, since they ignore the milling parameters: metal type (iron or steel), cut speed (0.25mm/rev or 0.5mm/rev), and cut depth (0.75mm or 1.5mm). Figure 14 shows the model’s anomaly confidence versus the flank wear for the 8 different milling configurations (using $\beta = 6$). We see there is, at best, a weak correlation between our predictions and flank wear in *aggregate* but a very strong correlation for each *individual* configuration. In fact, our anomaly confidence is physically interpretable: as the feed rate and depth increase (i.e., more material volume cut per revolution), the degree of flank wear corresponding to anomalous milling decreases.

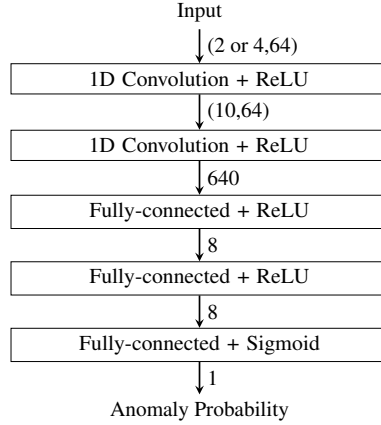


Figure 13. Model architecture for the milling DNNs, showing the input size to each layer.

B.3. Particle accelerator RF stations

We use the dataset constructed in (Humble et al., 2022) with additional transformations: (i) normalize the data, (ii) add $0.1 \times \mathcal{N}(0, 1)$ noise to each input, (iii) roll the BPM data between 0 and 10 points randomly, and (iv) select only the last 50 points in the RF data and the last 1000 in the BPM data. We define our algorithms $A_{\theta_s}, A_{\theta_q}$ as CNNs. As shown in Figure 15(a), our s network consists of two 1D convolutions with 5 out channels, kernel size 10, padding 0, and stride 1, followed by three FC layers of output size 6, 6, 1 respectively. As shown in Figure 15(b), our q network is very similar, using 15 out channels, a kernel size 20, and a stride of 5 instead. All layers but the final layer are followed by a ReLU activation. We train for 2000 epochs using a batch size of 400 and a train-test split of 85% – 15%. We use the Adam optimizer (Paszke et al., 2019) with a learning rate of 10^{-4} . We set $\alpha = 0.2$, which is the approximate anomaly rate based on the labels. We set $\lambda_{\text{wall}} = 1/\alpha$ and $\lambda_{\text{mag}} = 0$.

Coincident Learning for Unsupervised Anomaly Detection

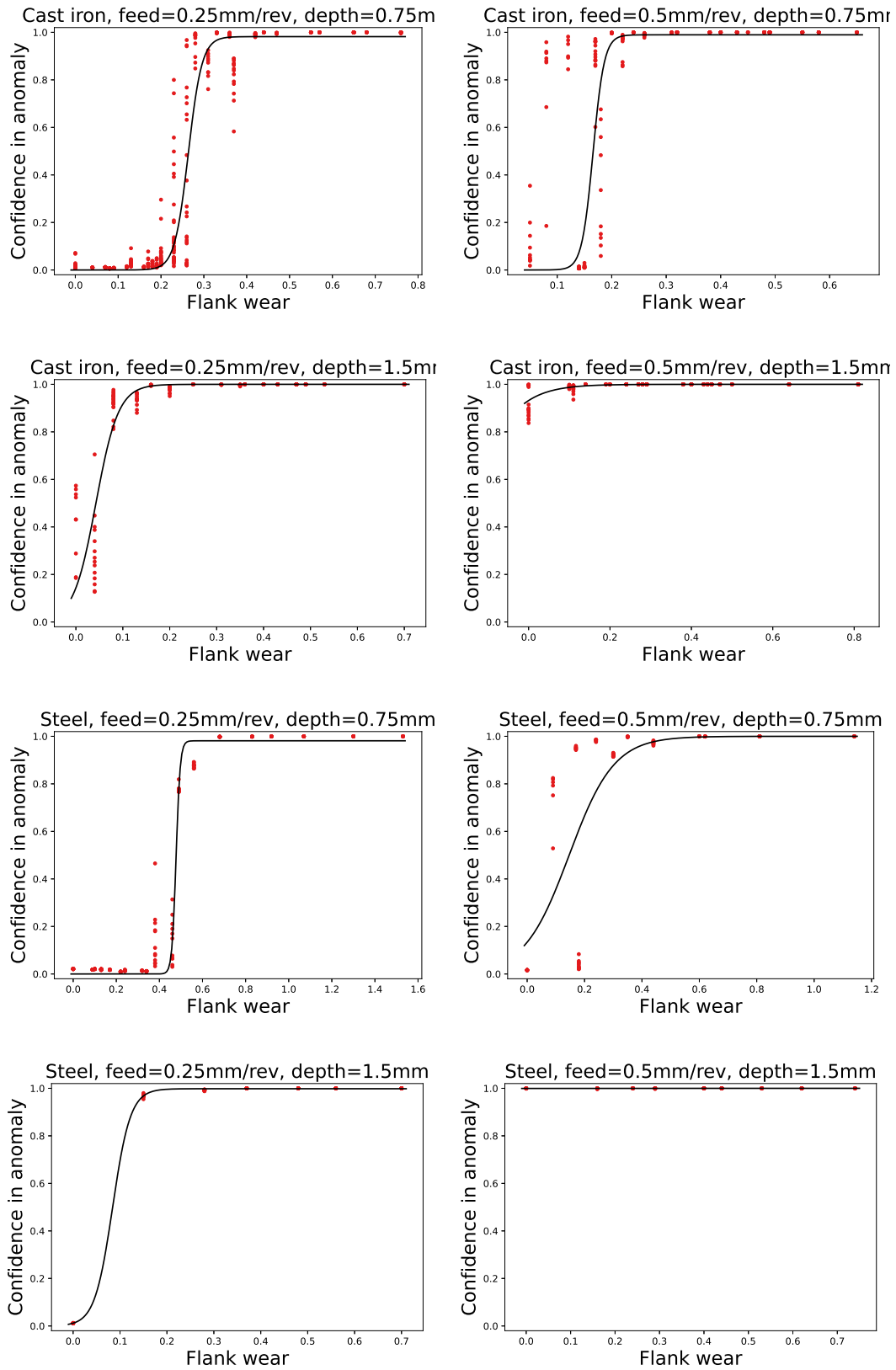


Figure 14. Anomaly probability versus flank wear for different milling configurations. Black line is a sigmoid fit.

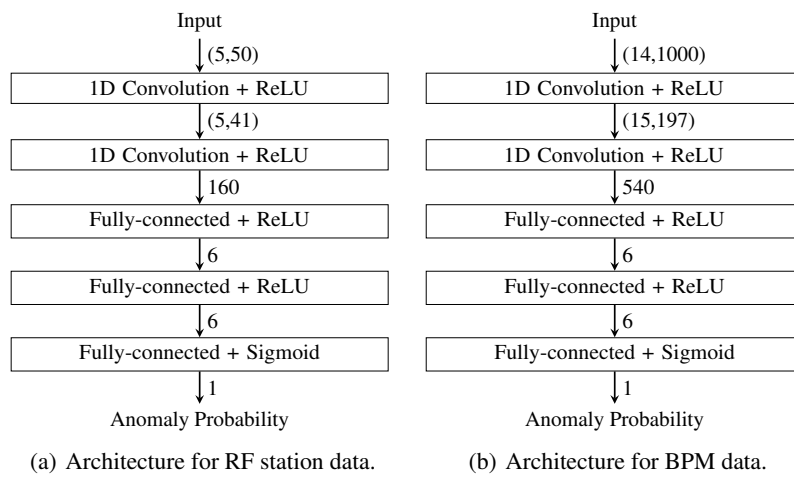


Figure 15. Model architecture for the particle accelerator DNNs, showing the input size to each layer.